Materials Horizons

ROYAL SOCIETY OF CHEMISTRY

REVIEW

View Article Online
View Journal | View Issue

Cite this: *Mater. Horiz.*, 2020, 7, 2596

Interfacial engineering of gold nanoclusters for biomedical applications

Yuvasri Genji Srinivasulu,[a] Qiaofeng Yao,[a] Nirmal Goswami[b] and Jianping Xie *[a]

Received 19th May 2020,
Accepted 16th July 2020

DOI: 10.1039/d0mh00827c

rsc.li/materials-horizons

Ultrasmall gold nanoclusters (Au NCs), with a particle size of ~1 nm, have recently emerged as a promising class of nanoparticles, due to their well-defined molecular formulae and structures, unique physicochemical properties (*e.g.*, optical absorption and photoluminescence), facile surface functionalization, and good biocompatibility. To explore the therapeutic potentials of these Au NCs, it is important not only to understand the interface between the NC surface and biological environment, but also to achieve desired biological functionalities *via* rational interfacial engineering. In this review article, we first describe the important biological considerations of Au NCs in their design for biomedical applications. We then aim to demonstrate diverse functionalization strategies of Au NCs to improve their physicochemical and biological properties. In the last section, we provide a detailed discussion on the applications of surface-engineered Au NCs in the fields of bioimaging, radiotherapy, photodynamic therapy, and antibacterial therapy, highlighting the important contributions of interfacial engineering of Au NCs to their biomedical applications.

1. Introduction

Atomically precise gold nanoclusters (Au NCs) are a promising class of functional nanomaterials, showing increasing potentials in both basic and applied research in the past two decades.[1–4] Recently, Au NCs have gained immense attention in the biomedical field, as bioimaging probes (for diagnosis),[5–7] radiosensitizers (for cancer radiotherapy),[8–10] photosensitizers (for photodynamic therapy),[11,12] and antibacterial agents (for combating infectious diseases).[13,14] The ultrasmall Au NCs, typically with a particle size of ~1 nm, possess distinctively different physicochemical properties from their larger counterparts – Au nanoparticles (NPs, with a particle size above 3 nm), including HOMO–LUMO transition,[15–17] quantized charging,[16,18] intrinsic chirality,[19–21] photoluminescence (PL),[22–24] and unique catalytic activity.[25–27] These unique physicochemical and biological properties are highly dependent on the size, composition, structure, and surface of the Au NCs.

[a] *Department of Chemical and Biomolecular Engineering, National University of Singapore, Kent Ridge, 117585, Singapore. E-mail: chexiej@nus.edu.sg*
[b] *Materials Chemistry Department, CSIR-Institute of Minerals and Materials Technology, Acharya Vihar, Bhubaneswar, Odisha-751013, India*

Yuvasri Genji Srinivasulu

Yuvasri Genji Srinivasulu received her B.E. (2013) from Anna University, India and her MSc (2014) from Nanyang Technological University (NTU), Singapore. She is currently pursuing her PhD in National University of Singapore (NUS), under the supervision of Prof. Jianping Xie. Her research focuses on interfacial engineering of gold nanoclusters using biomolecules for biomedical applications.

Qiaofeng Yao

Qiaofeng Yao received his B.S. (2010) from University of Science and Technology of China (USTC). He then earned his PhD (2015) from National University of Singapore (NUS), under the co-supervision of Prof. Jim Yang Lee and Prof. Jianping Xie. He is currently working as a Research Fellow with Prof. Jianping Xie at NUS. His current research interest focuses on developing total synthesis and self-assembly chemistry for atomically precise metal nanoclusters.

The physicochemical properties of the Au NCs can be rationally customized for diverse applications based on accurate structure–property relationship, which is made possible in an accelerating pace by recent progress on X-ray crystallography structure anatomy of Au NCs. In the past two decades, the synthetic chemistry of Au NCs, especially for those protected by thiolate ligands, has been significantly advanced, since the first successful attempt in synthesizing small thiolate-protected Au NPs by the Brust–Schiffrin protocol in 1994.[28] A number of efficient synthetic strategies, including bottom-up reduction-growth and cluster conversion, have been well-established in the past decade.[29–36] Many atomically precise Au NCs featuring a general molecular formula of $[Au_n(SR)_m]^q$ (where n, m, q represents gold atom number, ligand number, and the net charge of the cluster, respectively) have been successfully synthesized, by a delicate control of the reaction conditions, such as protecting ligands, reducing agents, ligand-to-metal ratios, solution pH, and temperature.[29,30,32,37–40] In addition, Au(I)-complexes and metastable NC intermediates have also been successfully identified during the evolution of the thermodynamically stable Au NC product, shedding fundamental light on the growth mechanism of Au NCs to realize their total synthesis.[41–43] The advances in atomically precise control in NC synthesis also enable successful crystallization of Au NCs, resolving their structures and finally elucidating their structure–property relationship.[44–48] With the help of X-ray crystallography, electrospray ionization mass spectrometry (ESI-MS) and advanced computational studies, a general structural scheme of thiolate-protected Au NCs has been revealed, where a typical $[Au_n(SR)_m]^q$ NC possesses one Au(0) core protected by a shell of staple-like $SR[Au(SR)]_x$ or cyclic $[Au(SR)]_x$ motifs (x = 0, 1, 2, 3...).[49] For example, recent experimental and theoretical efforts suggest a structural model for red-emitting $Au_{22}(SR)_{18}$ based on the core–shell structural scheme, where $Au_{22}(SR)_{18}$ consists of a Au_7 kernel surrounded by one cyclic $[Au_6(SR)_6]$ and three staple-like $[Au_3(SR)_4]$ motifs (Fig. 1a).[50] Such a structural model is in perfect agreement with the crystal structure of $Au_{22}(^t BuC{\equiv}C)_{18}$ NC ($^t BuC{\equiv}C$ denotes *tert*-butyl-acetylene), which was resolved recently by X-ray crystallography (Fig. 1b).[51]

Indeed, by leveraging on the structural insights of atomically precise Au NCs, researchers have exemplified various interfacial engineering approaches to rationally customize and improve their materials performance.[52–56] The interfacial engineering approach includes surface modification of Au NCs with different functionalities and self-assembly of Au NCs through their ligand shells. For example, through interfacial engineering, photoluminescence (PL), an important property of Au NCs that has been used for various biological applications such as biosensing and bioimaging, has been significantly improved.[57–65] In 2001, an interesting phenomenon known as aggregation-induced-emission (AIE) has been first coined by Tang's group to illuminate a non-emitting organic species through aggregation, by restricting their channel of non-radiative decay pathway.[66,67] The AIE concept has been adopted by our group in the system of thiolate-protected Au NCs to enhance their PL properties.[68,69] It should also be noted that the interface of Au NCs has a direct contact with the complex biological environment, and a good interfacial engineering of Au NCs is crucial for their further biomedical applications. Besides PL, the pharmacokinetic features of Au NCs inside the biological system, such as adsorption, distribution, metabolism, and excretion kinetics (ADME in short) are also highly dependent on the size, surface, and composition of the Au NCs.

In this review article, we first introduce the important biological considerations and their roles in designing functional Au NCs for biomedical applications. We then focus our discussions on the interfacial engineering approaches to tailor the physicochemical, as well as the physiological properties of Au NCs in the biological system. In the final section, we exemplify some recent applications of Au NCs in the biomedical field, such as biosensing, bioimaging, theranostics, and antibacterial therapy; highlighting the interfacial engineering principles of Au NCs in these applications.

Nirmal Goswami

Nirmal Goswami received his PhD (2014) degree from S. N. Bose National Centre for Basic Sciences, India, then pursued postdoctoral research at the National University of Singapore (2014–2017), and University of South Australia (2017–2019). He is currently a Scientist in the Materials Chemistry Department, CSIR-Institute of Minerals and Materials Technology (CSIR-IMMT), India. His research focuses on the interface between material science and biology.

Jianping Xie

Jianping Xie is currently an associate professor at the Department of Chemical & Biomolecular Engineering, NUS. He received his B.S. and M.S. in Chemical Engineering from Tsinghua University, China, and his PhD from the Singapore-MIT Alliance (SMA) program. He joined NUS in 2010 and established the BioNanoMetals research group. His group is known for their work on engineering ultrasmall metal nanoclusters for biomedical and environmental applications. His research interests include noble metal nanoclusters, nanomedicine, and applied environmental nanotechnology.

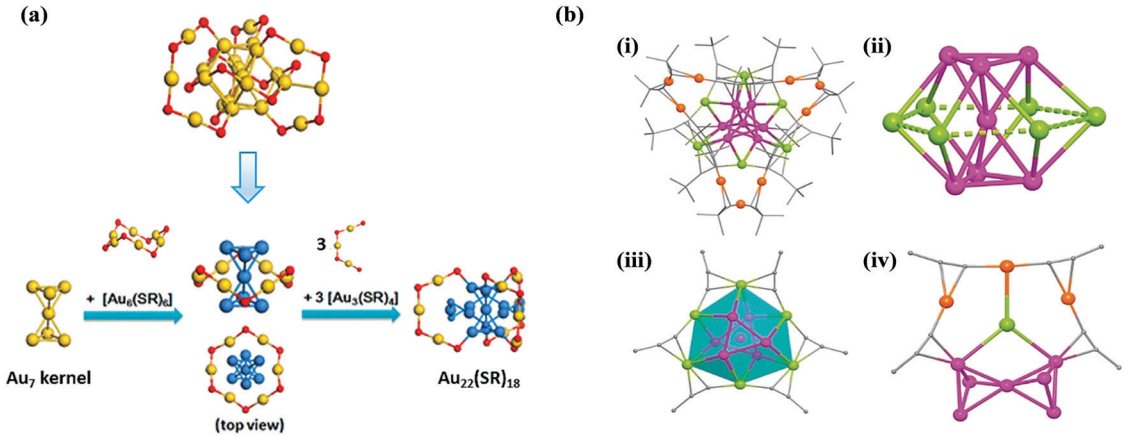

Fig. 1 (a) Proposed structural model of $Au_{22}(SR)_{18}$ consisting of a bi-tetrahedron Au_7 kernel surrounded by one cyclic $[Au_6(SR)_6]$ and three staple-like $[Au_3(SR)_4]$ motifs (sulphur atoms are shown in red and the rest are gold atoms; R group atoms are omitted for clarity). Reproduced with permission.[50] Copyright 2015, American Chemical Society. (b) (i) Molecular structure of $Au_{22}(^tBuC{\equiv}C)_{18}$ resolved by X-ray crystallography. $Au_{22}(^tBuC{\equiv}C)_{18}$ contains a Au_{13} kernel with six bridging alkynyl ligands in mid-section of Au_{13} kernel, and three $[Au_3(^tBuC{\equiv}C)_4]$ staples; (ii) Au_{13} cuboctahedron; (iii) Au_{13} kernel divided into Au_7 kernel and one $[Au_6(^tBuC{\equiv}C)_6]$ ring; (iv) the binding mode of one of the three staples $[Au_3(^tBuC{\equiv}C)_4]$ (carbon atoms are shown in grey and the rest are gold atoms). Reproduced with permission.[51] Copyright 2019, Wiley-VCH.

2. Biological considerations of Au NCs

A good design of functional nanomaterials for biomedical applications should have some primary features for their successful delivery to the biological systems. The key parameters that affect the fate of ultrasmall NPs or NCs in biological systems are size, structure, surface chemistry and composition.[70–72] Size is an important factor of functional NPs/NCs for their targeting, cellular uptake as well as clearance from the bloodstream. The effects of size of engineered NPs on their biodistribution are well-studied in the community. In particular, particles having a hydrodynamic diameter of $\sim$5.5 nm or less are considered as renally clearable NPs.[73,74] Being ultrasmall in size, Au NCs can not only accumulate to the target site through enhanced permeability and retention (EPR) effect but also be efficiently cleared from the body through kidney. Similarly, surface chemistry and composition also play a crucial role in determining their fate in the bloodstream, immune responses as well as their theranostic efficiency. In this section, we highlight the important biological considerations of the Au NCs for biomedical applications.

2.1. Protein–NCs interactions

When ultrasmall Au NCs were administered into the complex biological media (human blood plasma), several interactions would occur between the Au NCs and the macromolecules inside the body, such as proteins.[75] For Au NPs, it has been known that proteins will be adsorbed on the surface and form a so-called protein corona, which is often considered as a major problem for successful delivery of functional NPs to the target site.[76,77] In contrast to large NPs, ultrasmall NCs will react with the proteins differently. As Au NCs are in the same (or smaller) size range as the proteins, a one to one molecular interaction would occur.[78] Au NCs will bind to the specific sites of protein subunits and alter its conformation with less impact on its functionality. For example, a site specific complexation of *p*-mercaptobenzoic acid (MBA)-protected Au NCs on two allosteric sites of the thrombin with partial reduction in its activity has been demonstrated.[79] These interactions are reversible or irreversible depending on the adsorption kinetics and thermodynamic stability of the protein–NC complexes formed.[80,81] Recently, it has been demonstrated that Au NCs of the same core size and surface charge but protected by two different ligands (MBA and glutathione (GSH)) possess different association rate constants with proteins.[82] MBA-protected Au NCs (referred to as MBA-Au NCs) exhibited fast diffusion-limited adsorption with larger association rate constant compared to the slow, reaction-limited adsorption of GSH-protected Au NCs (referred to as GSH-Au NCs). These observations agree well with an earlier study on the dynamic reversible interactions of GSH-Au NCs with three dominant serum proteins (human serum albumin, gamma-globulins, and transferrin).[83] This type of reversible interactions help maintain the hydrodynamic diameter of Au NCs in blood plasma. As a result, GSH-Au NCs were excreted rapidly through renal clearance pathway.[84] On the other hand, MBA-Au NCs were found to accumulate in liver and spleen for longer time. These differences are mainly attributed to the changes in surface charge distribution and hydrophobicity of the Au NCs.

2.2. *In vivo* distribution and cellular uptake

Cellular uptake determines the performance of the NPs as therapeutic or theranostic agents. Long circulation or blood retention time is highly desirable for better cellular uptake of the NPs.[85] Surface charge of NPs plays a dominant role in sub-organ distribution and intracellular uptake.[86] It is well known that neutrally charged NPs such as PEGylated NPs (PEG denotes polyethylene glycol) possess longer circulation half-life in blood with negligible protein opsonization, aggregation and phagocytosis.[87] PEGylation is therefore a most common and

successful surface modification strategy of inorganic NPs to improve their blood circulation time. Even in the cases of NCs, PEGylation of Au NCs was found to improve their tumor targeting capability compared to the zwitterionic Au NCs (GSH-Au NCs).[88] Besides accumulation on the target sites, internalization of PEGylated/GSH Au NCs into the tumor cells is relatively low.[89,90] Recently, significant uptake of GSH-Au NCs into human cervical carcinoma HeLa cells was achieved by adding cysteamine (Cystm) moiety on the surface of Au NCs. The protonation of cysteamine in acidic tumor microenvironment (~pH 6.5) enabled interaction of GSH-Cystm-Au NCs with the negatively charged tumor cell membrane, thereby enhancing their uptake.[91]

Hydrophobicity of surface ligands also determines the lifespan of the NCs in bloodstream. It has been observed that inclusion of oligo ethylene glycol (OEG) moieties on the surface of GSH-Au_{25} NCs increased their circulation half-life by decreasing its elimination half-life.[92] As more and more hydrophobic moieties were added on the surface of ligands, the pharmacokinetics of Au NCs were changed.[93] A detailed analysis of the impact of hydrophobic ligands on the cellular uptake process was studied recently by Porret *et al.*[94] It was demonstrated that Au NCs stabilized by the customized zwitterionic ligands with varying degree of hydrophobicity can prevent the formation of protein corona and control their insertion into the phospholipid membrane and their final cellular uptake.

Internalization of the NPs into cells depends on several mechanisms, such as phagocytosis, pinocytosis, and receptor-mediated endocytosis.[95] The choice of endocytic pathway depends on the size and surface chemistry of NPs/NCs. As Au NCs are in <2 nm regime, they would form clusters of NCs on the surface of cell membrane to initiate the endocytosis process.[96] This process is different from that was observed in large NPs. Therefore, clustering of NCs can be an efficient strategy to improve both the circulation time and cellular internalization of functional NCs.

2.3. Renal clearance

Zwitterionic NCs, especially GSH-protected Au NCs, are marked for their exceptional renal clearance property.[84,97,98] Being ultrasmall in size, even few atom differences in Au NCs may lead to significant changes in their renal clearance profile. Recently, Du *et al.* found that GSH-protected Au_{10-11}, Au_{15}, and Au_{18} NCs were retained in the glomerular glycocalyx for longer time compared to Au_{25} NCs.[99] This is because the glomerular barrier acts as a size band pass filter rather than a size cut-off filter for sub-nanometer NCs.[100] Besides the differences in their atomic number, surface ligand composition and surface charge also have pronounced impact on the renal clearance of Au NCs. The effect of ligand length on efficient renal clearance of peptide-protected Au NCs were studied by Ning *et al.*[101] They synthesized cysteine (Cys)-protected and glycine–cysteine (Gly–Cys)-protected Au NCs of the same core size with a slight difference in their hydrodynamic diameter (2.3 ± 0.4 nm). An increase in single amino acid from cysteine to glycine–cysteine has increased their colloidal stability in the physiological conditions with enhanced renal clearance. The renal clearance efficiency of Gly–Cys-Au NCs is 41.6% injection dose (ID), which is nearly two-fold higher than the Cys-Au NCs (~21.5% ID) and it is comparable to GSH-Au NCs (~50% ID) at 24 h post injection.

The effect of surface charge on the renal clearance of Au NCs is substantiated by Yu *et al.*[91] The inclusion of cysteamine moieties on the surface of GSH-Au NCs (GSH-Cystm-Au NCs) has decreased their zeta potential from −48.0 mV (GSH-Au NCs) to −22.1 mV (GSH-Cystm-Au NCs). Decreased surface negative charges of GSH-Cystm-Au NCs has reduced their renal clearance efficiency (~10% ID) compared to GSH-Au NCs (~28% ID) at 1 h post intravenous injection. This highlights the importance of surface chemistry of Au NCs on their renal clearance efficiency.

3. Interfacial engineering of Au NCs

The biomedical applications of Au NCs are mainly driven by their size, functionality, and physicochemical properties. However, it is often difficult to maintain those features in biological environment due to the obstacles mentioned in the above section. In this section, we discuss various interfacial engineering strategies that can help retain or enhance both physicochemical and physiological properties of Au NCs in biological environment.

3.1. Interfacial engineering of Au NCs by choice of ligands

Au NCs with well-defined structure and function can be achieved by selecting the appropriate ligands. Since ligand shell will be the first layer of the Au NCs to interface the biological environment, the nature of the surface ligands or the surface chemistry of NCs will determine the types of proteins interacting with the NCs, strength of the interactions, and their further interactions with cells or cell components. In the last few years, there are a number of successful attempts in designing the biocompatible ligands such as thiol-based molecules, peptides, proteins, polymers, and dendrimers, demonstrating the potentials in using biocompatible ligands to prepare Au NCs with the desired attributes.

3.1.1. Small thiol-based molecules. Thiolate ligands have been used for decades as protecting agents of Au NPs due to their strong covalent bond with gold.[102] The thiol (–SH) group of organic ligands or peptides will interact with Au^{3+} ions to form thiolate–Au(I) complexes.[103,104] Well-defined Au NCs can be produced by controlled reduction of these thiolate–Au(I) complexes. As the surface chemistry of the NCs plays a major role in improving their biological interactions, protocols have been developed to prepare various thiolate-protected Au NCs. For example, we have developed a sodium hydroxide (NaOH)-mediated sodium borohydride ($NaBH_4$)-reduction protocol, through which one can not only obtain well-defined Au NCs but also vary their surface functional groups (Fig. 2a).[105] In this protocol, NaOH was used to decrease the reducing power of $NaBH_4$ (slow down the rate of the forward reaction) and to

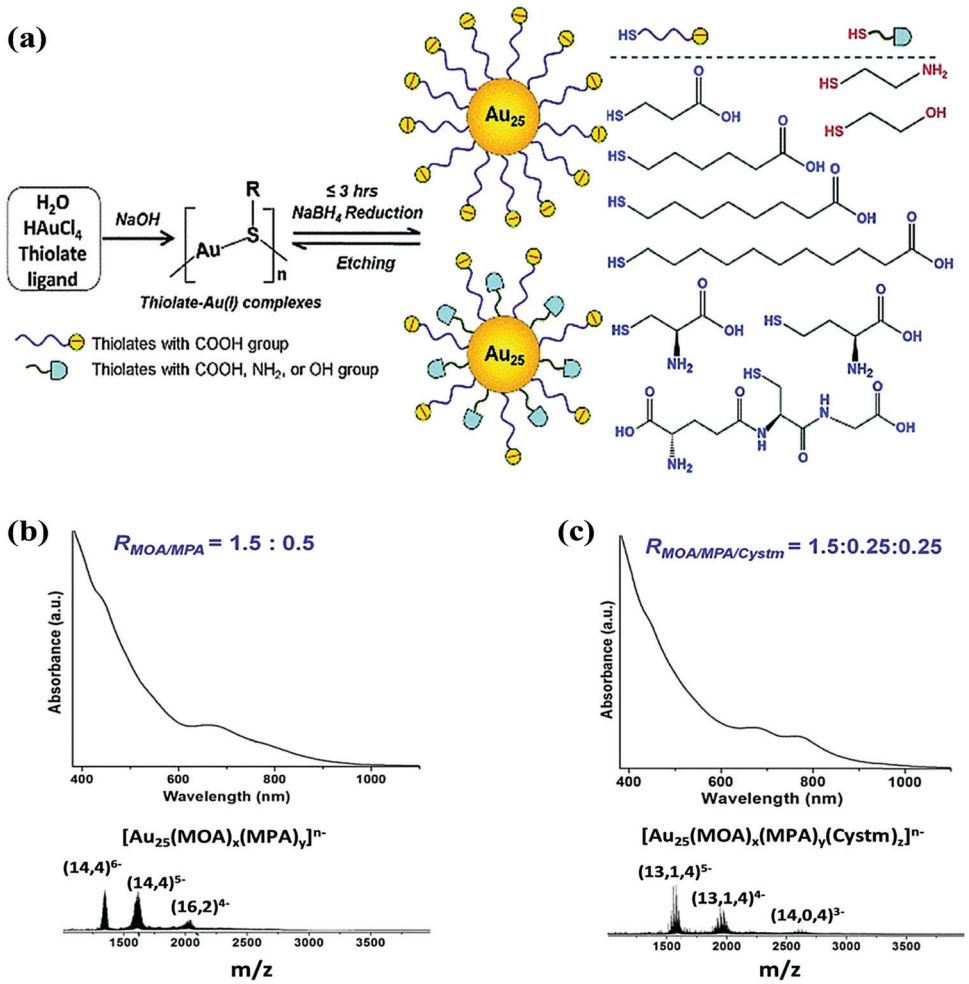

Fig. 2 (a) Schematic illustration of NaOH-mediated $NaBH_4$-reduction protocol for the synthesis of thermodynamically stable thiolate-protected Au_{25} NCs. (b) UV-Vis absorption (top) and ESI mass (bottom) spectra of the as-synthesized bi-thiolate-protected Au_{25} NCs. (c) UV-Vis absorption (top) and ESI mass (bottom) spectra of the as-synthesized tri-thiolate-protected Au_{25} NCs (here MOA denotes 8-mercaptooctanoic acid; MPA denotes 3-mercaptopropionic acid; and Cystm denotes cysteamine). Reproduced with permission.[105] Copyright 2014, Wiley-VCH.

increase the etching capability of thiolate ligands (push up the rate of the backward reaction), the balance of which can lead to the formation of a thermodynamically stable Au_{25} NC in a short reaction time (3 h or less). Bi- or tri-thiolate ligand-protected Au_{25} NCs can also be produced by controlling the feeding ratio of thiolate ligands, as shown in Fig. 2b and c. Therefore, a surface coverage of Au NCs with rich functional moieties can be obtained in a facile and scalable manner through our method, providing an efficient platform for further surface modification of Au NCs for biomedical applications.

Bi-dentate and multi-dentate ligands (*i.e.*, ligands with multiple thiol groups) can improve the colloidal stability of Au NCs in the complex biological media. For instance, bi-dentate lipoic acid functionalized Au NCs were found to be stable in plasma for weeks.[106,107] To improve their circulation time and cellular uptake in the serum-rich media, Porret *et al.* have designed $ZwMe_2$, $ZwEt_2$, ZwBuEt, and $ZwBu_2$ ligands in the order of increasing hydrophobicity (Zw: zwitterion conjugated lipoic acid moiety; Me_2: methyl amide linkage; Et_2: ethyl amide linkage; BuEt: butylethyl amide linkage; Bu_2: butyl amide linkage) to synthesize Au NCs (Fig. 3a).[94] The hydrodynamic diameter of the Au NCs was maintained well below the renal clearance threshold. It was evident that the higher the hydrophobicity of the ligand, the better is their colloidal stability in the serum-rich media with improved cellular uptake. Penetration of the hydrophobic Au NCs into the phospholipid bilayer of cell membrane was mainly due to their shift from more negative zeta potential to a neutral one as the hydrophobicity of the Au NCs increased. Additionally, PL enhancement toward near-infrared (NIR) region (λ_{em} = 780 nm, λ_{ex} = 500 nm) was also observed by simply changing the methyl amide group to the ethyl amide group. However, further increase in hydrophobic chain lengths has decreased their PL quantum yield and increased their cytotoxic effects (Fig. 3b).[94] These results indicate that a fine balance between hydrophilicity and hydrophobicity of the surface ligands of Au NCs is an important consideration for their biomedical applications.

3.1.2. Proteins. Bio-macromolecules, such as proteins or DNA, can act as templates or multi-dentate ligands for the formation of Au NCs. Use of these macromolecules as

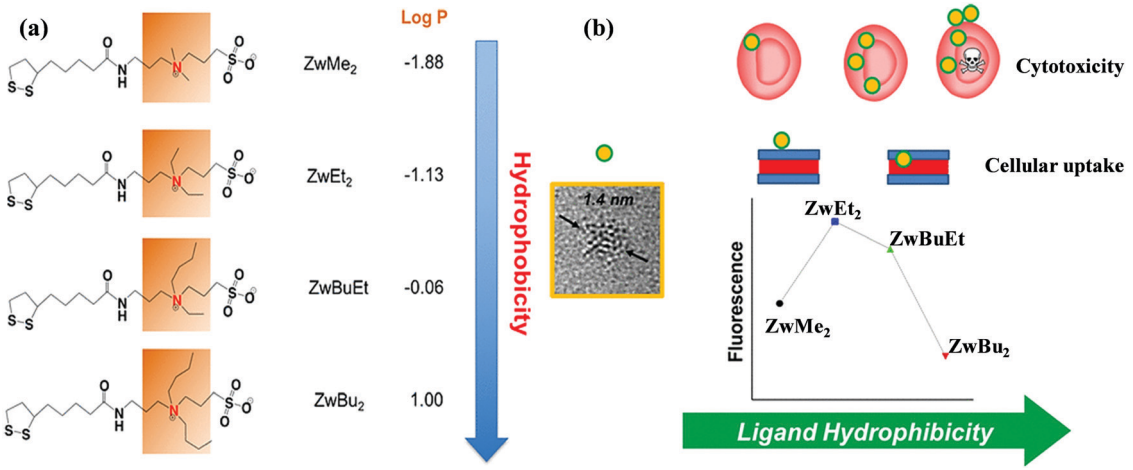

Fig. 3 (a) Schematic illustration of the thioctic zwitterion molecules (Zw) synthesized using different amide precursors. log *P* value depicts the degree of hydrophobicity. (b) Schematic illustration of how the increase in ligand hydrophobicity of Au NCs affects both their physicochemical and physiological properties. Reproduced with permission.[94] Copyright 2017, American Chemical Society.

protecting ligands is advantageous due to their tunable amino acids or nucleotide sequences, rich functional chemistry, and good biocompatibility. In particular, proteins gained immense attention for the synthesis of Au NCs after the pioneering work by Xie *et al.*[108] A biomineralization approach was designed to reduce gold salts within the protein scaffold by utilizing its intrinsic reducing moieties (side groups of tyrosine and tryptophan). Under mild reaction conditions (at physiological temperature of 37 °C and the solution pH was adjusted to ~12), bovine serum albumin (BSA)-protected Au NCs with strong red emission at 640 nm (λ_{ex} = 470 nm, PL QY ~6%) have been successfully synthesized (Fig. 4a). The strong Au–S bonds provided by the cysteine residues of BSA template in combination with good steric protection of the bulky BSA molecule, enhanced their stability in extreme conditions (high salt concentrations, different pH, and various buffers), facilitating the *in vitro* and *in vivo* biomedical applications of BSA-protected Au NCs.[108] Since then, many interesting works on protein-directed synthesis of noble metal NCs were reported. For example, a BSA-based hydrogel network encompassing Au NCs was synthesized by slightly increasing the pH and temperature. High resolution transmission electron microscopy (HR-TEM) confirmed the *in situ* formation of Au NCs within the hydrogel network. The shear thinning with moldable feature of the hydrogel was observed without compromising the NC luminescence.[109] Besides serum proteins, many other proteins such as lysozyme,[110] pepsin,[111] insulin,[112] and globulins,[113] have also been used to synthesize Au NCs.

Rational design of proteins is highly recommended for the sustainable synthesis of Au NCs. Insertion of pre-defined cluster coordination sites into the protein scaffold was recently reported to control the synthesis of Au NCs. For example, Aries *et al.* have customized the consensus tetratricopeptide repeat (CTPR3) protein by inserting two histidine (H in short) residues to the protein concave surface (so-called H module).[114] Histidine residues act as cluster coordination sites due to their strong affinity toward noble metals (such as Au in 0 and +1 oxidation state). By combining the H module with the wild type CTPR3-repeat protein (W) module, three different proteins CTPR3-WWW, CTPR3-HWW, and CTPR3-WHW were designed

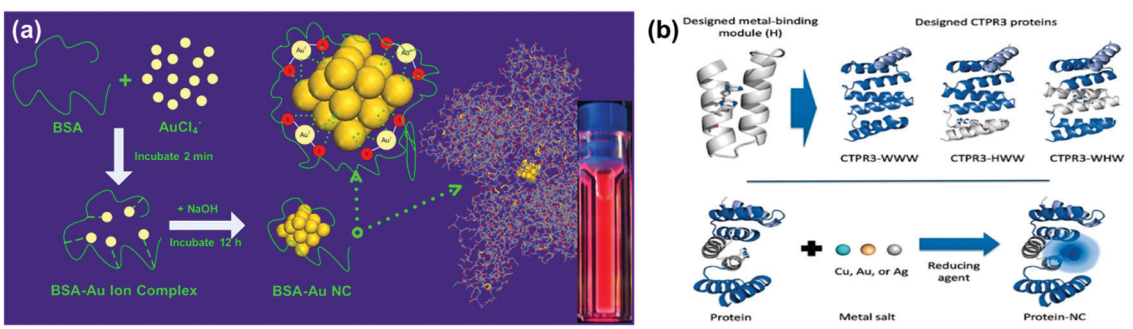

Fig. 4 (a) Schematic illustration of protein-directed synthesis of Au NCs. Reproduced with permission.[108] Copyright 2009, American Chemical Society. (b) Top panel: rational design of CTPR protein by inserting two histidine residues at position 5 and 9, termed as H module. Combination of the H module with W modules of CTPR protein, three different proteins (CTPR3-WWW, CTPR3-HWW, and CTPR3-WHW) were designed. Bottom panel: schematic illustration of designed proteins with metal salts and reducing agent for the formation of protein-stabilized NCs (Protein–NC). Reproduced with permission.[114] Copyright 2019, Wiley-VCH.

and further used as templates for Au NC synthesis (Fig. 4b). While a PL QY of 8.3% was obtained for CTPR3-WHW-protected Au NCs, negligible PL was observed for other two protein-protected NCs. This highlights the significance of the strategic placement of histidine residues on the protein template in improving their physicochemical properties. Additionally, the structural integrity of CTPR3-WHW protein was retained after the synthesis of Au NCs.[114] Retaining the structural integrity of proteins in protein-stabilized Au NCs is important when these Au NCs were administered into the biological systems. Any conformational change could alter the function of proteins, triggering the immune response for phagocytic uptake and thereby leading to long term accumulation and liver necrosis.[115–118]

3.1.3. Polymers and dendrimers. In addition to biomolecules, biodegradable polymers and dendrimers have also been used to synthesize Au NCs. Polyethylene glycol modification (PEGylation) is the most common strategy to impart the stealth property (high level of hydration of the hydrophilic polymer backbone that prevents protein opsonization and improves the systemic circulation) to functional NPs.[87] By optimizing the PEGylation chemistry and extent of PEGylation, physicochemical properties of PEGylated Au NCs can be improved for their desired applications. For instance, Aldeek *et al.* have appended a series of functional PEG moieties to bidentate lipoic acid to serve as ligands in the formation of Au NCs.[107] By controlling the molar fractions of gold precursors and ligands, Au NCs with rich surface coverage have been obtained, showing improved colloidal stability and enhanced PL properties. Rich functional groups on the surface of polymers enabled the formation of micelles or hybrid structures. Recently, thiolated diblock co-polymer (PEG–PNIPAm-SH), consisting of hydrophilic PEG block and thermosensitive poly(*N*-isopropyl acrylamide) (PNIPAm) block, has been used as a stabilizer to form gold–polymer nanohybrids. When temperature was above the lower critical solution temperature (LCST) of PNIPAm, a stable micelle structure with enhanced PL emission (λ_{em} = 720 nm, λ_{ex} = 550 nm) in NIR-I window was observed (Fig. 5a).[119] Other polymers, such as poly(*N*-vinyl pyrrolidone) (PVP),[120] and polyethyleneimine (PEI),[121] have also been used to prepare luminescent Au NCs.

Dendrimers, a unique class of polymers with well-defined branched architecture, can also serve as templates for *in situ* formation of Au NCs.[122] Besides being a passivating molecule, dendrimers provide immense functionalities in improving the physicochemical properties of the encapsulated Au NCs. For example, Zheng *et al.* was the first to use dendritic polymer, poly(amidoamine) (PAMAM), to prepare blue-emitting Au_8 NCs.[123] By stoichiometric mixing of gold salt precursors and dendrimers, gold ions can aggregate in the dendrimer cavity and they can be reduced slowly by an equivalent amount of $NaBH_4$ to form both Au NCs and large Au NPs. The Au NCs were highly luminescent with a QY of ~41%, which is significantly higher than those Au NCs protected by thiolate ligands.[6] The monodispersity of the Au NCs can be controlled by the generation of dendrimers, gold ion concentration, and the reducing strength of the reaction system.[124] Recently, time-course measurements were performed to unravel the formation mechanism and the origin of PL of PAMAM-ligated Au_5 NCs (poly-Au_5).[125] A two-stage growth process was revealed, including stage I of self-nucleation and self-assembly with rapid increase in PL, and stage II of sole self-assembly with slow increase ($\leq$30%) in PL of Au NCs within PAMAM dendrimer (Fig. 5b). An intense emission of poly-Au_5 at 458 nm with QY of 25% was attributed to two major reasons: (1) self-assembled NCs within PAMAM dendrimer can enhance the ligand-to-metal-to-metal charge transfer (LMMCT) from the electron-rich amine ($-NH_2$) of PAMAM to Au atoms; and (2) poly-Au_5 also possesses enhanced aurophilic interactions, which can further promote its excited-state relaxation dynamics.[60,130] Additionally, poly-Au_5 nano-assemblies were found to be biocompatible with good bio-stability in strong oxidizing and reducing intracellular environment.[125]

3.2. Interfacial engineering of Au NCs by ligand exchange reaction

Surface functionality can be tailored by another dynamic process known as ligand exchange reaction. In 1999, Hostetler *et al.* have introduced this strategy to add new functionalities to the alkane thiolate-protected Au NCs.[126] This reaction requires excess amount of incoming ligands to replace the original

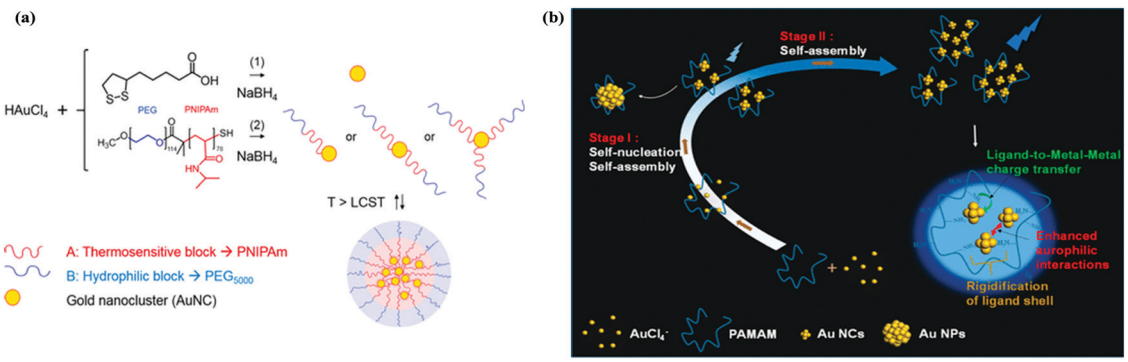

Fig. 5 (a) Schematic illustration of *in situ* formation of Au NCs using (1) lipoic acid and (2) thiol-terminated thermosensitive PEG–PNIPAm-SH polymer, as ligands. The micelle formation of polymer-stabilized Au NCs upon heating above the lower critical solution temperature (LCST) is also shown. Reproduced with permission.[119] Copyright 2018, American Chemical Society. (b) Schematic illustration of two-stage growth process of PAMAM-ligated poly-Au_5 nano-assemblies with their intense blue emission under UV irradiation. Reproduced with permission.[125] Copyright 2018, American Chemical Society.

ligands on the ligand shell of NCs. Based on the concentration of the incoming ligands and reaction parameters, either complete or partial ligand exchange can take place according to the following reaction:

$$x(R'SH) + Au_n(SR)_m \rightarrow x(RSH) + Au_n(RS)_{m-x}(R'S)_x$$

where x and m denote the number of the incoming (R′SH) and the original (RSH) alkane thiolate ligands, respectively.[126] Through complete ligand exchange reaction, structural transformation of parent NCs was also possible. For example, Shichibu *et al.* have reported complete size and structural transformation of phosphine-stabilized Au_{11} NCs to GSH-protected Au_{25} NCs with good monodispersity and high yield.[127] The mechanism of ligand exchange induced structural change of parent NCs was later proposed by George *et al.*[128] They used bulky incoming ligand 4-*tert*-butylbenzenethiol (TBBT) to exchange phenyl ethane thiol (PET) of PET-stabilized Au_{25} NCs. As TBBT is bulkier than PET, such ligand exchange reaction transformed the icosahedral Au_{25} NCs to the bi-tetrahedron Au_{22} NCs. The transformation process and intermediate structures of this ligand exchange reaction were also tracked by time dependent matrix assisted laser desorption ionization-mass spectrometry (MALDI-MS).[128] Besides size and structural transformation of parent NCs, selective functionalization of ligand shell is also possible by controlling the nature and concentration of the incoming ligands. For example, Shibu *et al.* have carefully modified the optical properties of GSH-protected Au_{25} NCs by a ligand exchange with thiol-containing 2-mercapto-butanol (MB) (Fig. 6).[33] The exchanged product, with negligible change in their core structure, possesses enhanced PL QY in solid state compared to their parent NCs.

3.3. Interfacial engineering of Au NCs by clustering of NCs to NPs or nanohybrids

A large number of ligands with various functional groups have been employed either in the synthesis of Au NCs or in the ligand exchange reaction. The functionality of these NCs was often enriched by formation of nanohybrids with other functional NPs. Such functional nanohybrids or NPs can be formed *via* either non-covalent or covalent interactions.

3.3.1. Non-covalent interactions. Towards the goal of enhancing the PL of Au NCs, a series of strategies have been designed. Aggregation-induced-emission (AIE) through ligand shell engineering is one such strategy that has gained immense attention in recent years.[129–131] Besides AIE-type Au NCs,[68] the PL of non-AIE-type NCs can also be improved by rigidifying the ligand shells of Au NCs. For example, silver ions were used to bridge the staple motifs in the protecting shell of GSH-protected Au_{18} NCs. Through this approach, the PL QY of the NCs was increased from 0.37% to ~6.8%.[132] Similarly, some efforts on ligand shell rigidification of Au NCs were also reported.[133–135] Though PL QY of Au NCs was improved, rapid clearance with short circulation half-life was still one of the major concerns of ultrasmall Au NCs for *in vivo* applications. To improve their *in vivo* biodistribution, clustering of NCs to NPs or nanohybrids was found to be an efficient approach. The formation of nanohybrids/NPs through non-covalent interactions by adopting either self-assembly or host–guest recognition approaches are explained below.

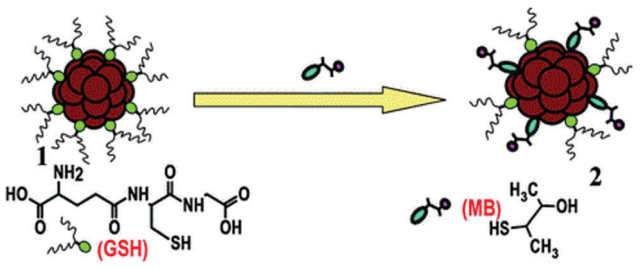

Fig. 6 Schematic illustration of ligand exchange reactions of GSH-protected Au_{25} NCs **1** with 3-mercapto-2-butanol (MB), producing **2** by the incorporation of MB in the ligand shell of **1**. Reproduced with permission.[33] Copyright 2008, American Chemical Society.

3.3.1.1. Self-assembly. Spontaneous association of functional molecules into a structurally well-defined aggregate through non-covalent bonds is termed as self-assembly.[136] Self-assembly occurs at all scales, and biology has numerous self-assembled nanostructures (*e.g.*, DNA macromolecules). A diverse range of non-covalent interactions, such as electrostatic interactions, hydrogen bonding, hydrophobic interactions, van der Waals forces, and dipole–dipole interactions, can be used to stabilize the nanostructures.[137,138] Such a powerful approach is becoming an emerging strategy in cluster community for the formation of nanohybrids/NPs with improved physicochemical and physiological properties. As Au NCs can act as nano-ions, electrostatic interactions between surface ligands of Au NCs and macromolecules can play a dominant role during the self-assembly process in aqueous media. For example, our group have applied a cationic polysaccharide, namely chitosan of medium molecular weight, to self-assemble ultrasmall negatively charged GSH-Au NCs.[139] By optimizing the parameters such as molar ratio of chitosan and NCs, solution pH, temperature, and reaction time, a highly luminescent Au NCs-impregnated nanogel was obtained. These nanogels were about 200 nm in size (hydrodynamic diameter), and showed ~3.7-fold increase in PL compared to Au NCs without chitosan (Fig. 7a(i) and (ii)). The presence of Au NCs within the chitosan nanogel was evident from the TEM images (Fig. 7a(ii)). The reason for PL enhancement of Au NCs-impregnated nanogel is the spatial confinement of Au NCs within the nanogel matrix (Fig. 7a(iii)–(v)).[139] In addition to the enhanced PL, the as-formed nanogel might also increase the acceptance of Au NCs in bioimaging and other biomedical applications, as they could elongate the circulation lifetime of Au NCs in the biological system. Another biocompatible cationic polymer, namely poly(allylamine hydrochloride) (PAH), was also used for the self-assembly of ultrasmall GSH-Au NCs. The as-synthesized nanogel possessed pH-based swelling–shrinking property, extending their utilization as stimuli-responsive drug nano-carriers.[140]

Besides polymers, ultrasmall Au NCs can also be encapsulated into porous materials, such as metal–organic framework (MOF)[141,142] and mesoporous silica NPs.[143,144] For example, GSH-Au NCs were aggregated in the presence of weakly polar

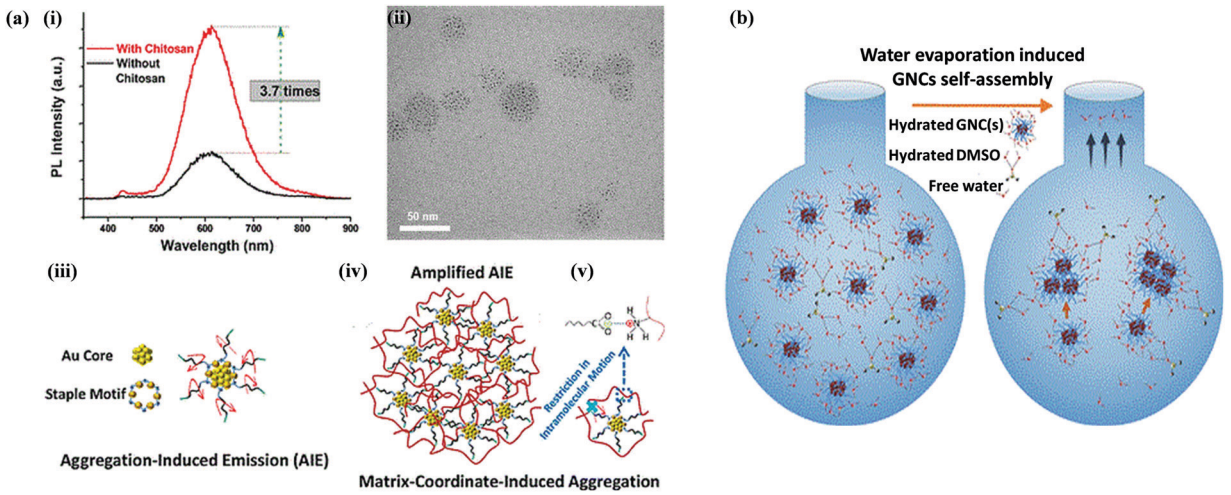

Fig. 7 (a) Formation of highly luminescent thiolated Au NCs self-assembled in nanogel. (i) Comparison of PL intensity of GSH-Au NCs with (red) and without (black) chitosan; (ii) TEM image of the as-formed nanogel; (iii) schematic illustration of individual AIE-type GSH-Au NCs, where the outer surfaces of ligands are free to rotate or vibrate in solution; (iv) GSH-Au NCs within chitosan nanogel, showing amplified AIE through matrix-coordination; (v) electrostatic interaction between negatively charged inidividual GSH-Au NCs and positively charged chitosan, restricting their rotational or vibrational motion in solution. Reproduced with permission.[139] Copyright 2016, American Chemical Society. (b) Schematic illustration of water evaporation induced Au NCs self-assembly process in a water-DMSO binary solvent. Reproduced with permission.[146] Copyright 2018, American Chemical Society.

solvents (*e.g.*, methanol, ethanol, and isopropanol), leading to the formation of aggregated Au NCs. Based on the AIE phenomenon, the aggregated Au NCs showed higher PL intensity. To further enhance the stability of the aggregated Au NCs in biological environment, they were encapsulated into MOF (zeolitic imidazolate framework-8 (ZIF-8)) by coordination-induced self-assembly (interaction between Zn^{2+} ions and organic ligands of Au NCs). Due to the pH-dependent dissociation of ZIF-8 matrix, the aggregated Au NCs were released under the acidic pH (endosomes/lysosomes, where pH is ~5–6) for real-time monitoring of intracellular events.[141]

As discussed above, cellular internalization is an important aspect in biomedical applications. Higher internalization leads to better performance of the therapeutic material. The commonly known cellular internalization pathways are phagocytosis, macro- or micro-pinocytosis, and receptor-mediated endocytosis. Inspired by the invasion of pathogens into the host cells through macro-pinocytosis,[145] Zhang *et al.* have constructed a template-free assembly of GSH-protected Au_{22} NCs as super-gold NC assemblies (SGNCs).[146] By simply evaporating water molecules in a binary solvent mixture containing water and dimethyl sulfoxide (DMSO) or by dialyzing the GSH-Au_{22} NCs against DMSO, dynamic intermolecular hydrogen bond interactions between GSH-Au NCs and mixed solvent were controlled to form micro to meso scale assemblies (Fig. 7b). Addition of folic acid moiety to SGNCs enabled their entry into cancer cells through macro-pinocytosis in a receptor-dependent manner similar as viral pathogens.[146] The presence of rich surface functional moieties on the NC surface serves as a promising class of building blocks to scale up into superstructures for biomedical applications.

3.3.1.2. Host–guest chemistry. Host–guest chemistry describes the complexation of guest molecules by the host molecules in a highly controlled and cooperative manner.[138,147] Host–guest complexation is abundant in nature, such as antigen–antibody interactions, receptor–ligand binding, enzyme–substrate selectivity, and carbohydrate–protein complexes. This specific, dynamic, bio-orthogonal chemistry provides a powerful paradigm of supramolecular chemistry by serving as building blocks of hierarchical nanostructures.[148,149] The most common host–guest pair for biomedical applications (*e.g.*, biosensing and bio-labelling) is biotin–avidin pair.[150,151] For example, Chen *et al.* have designed biotin–avidin complexation to form Au NCs-based dual emission fluorescent NPs (DEFNs).[152] Biotinylated Au NCs were decorated on the surface of streptavidin-modified silica NPs, forming a crown-like NP assembly. The high association constant, K_a ($K_a = 10^5\ M^{-1}$) of biotin–avidin pair through multiple non-covalent interactions (*e.g.*, hydrogen, hydrophobic, and van der Waals forces) improved the stability of DEFNs even in those serum-rich media. In a separate work, the lock and key principle of this biotin–avidin pair enabled self-assembly of avidin-modified Au NCs on the biotinylated cancer cell membrane for the amplified detection of cancer cells.[153]

Host–guest chemistry also provides a good design platform for thiolate-protected Au NCs as a drug carrier. Recently, Li *et al.* have synthesized pentapeptide (GSHaa, where aa is D-alanine–D-alanine termini) protected Au NCs to load vancomycin (an antibiotic drug against Gram-positive bacteria) on its surface.[154] By utilizing the specific monovalent host–guest interaction of vancomycin with the terminal peptide D-alanine–D-alanine of GSHaa-Au NCs ($K_a = 2.67 \times 10^4\ M^{-1}$), efficient loading of vancomycin was reported.[154,155] Besides monovalent host–guest system, multivalent host molecules such as β-cyclodextrin (β-CD) can also be conjugated to the surface of Au NCs.[156,157] β-CD is a cyclic oligosaccharide with a

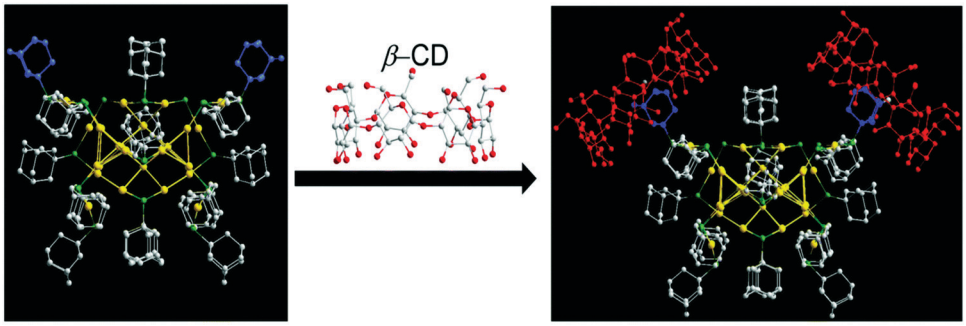

Fig. 8 Schematic illustration of formation of $Au_{38}S_2(SAdm)_{20} \cap (\beta\text{-CD})_2$ conjugate. The host–guest interaction of β-CD with adamantane ligands is shown in red and blue (right side of the arrow). Other adamantane ligands are shown in white (left side of the arrow). Gold atoms are shown in yellow, sulphur atoms in green, carbon atoms in white and blue, and oxygen in red. All hydrogen atoms are omitted for clarity. Reproduced with permission.[159] Copyright 2016, Royal Society of Chemistry.

hydrophobic inner cavity and hydrophilic exterior, which possesses specific binding to various guest molecules (*e.g.*, adamantane, azobenzene, cholesterol, and ferrocene), forming a stable host–guest complex.[158] For example, Yan *et al.* have synthesized adamantane–thiolate-protected Au NCs ($Au_{38}S_2(SAdm)_{20}$, where –SAdm is adamantane–thiolate ligand), which showed specific binding toward β-CD compared to α-CD or γ-CD.[159] Two of the adamantane ligands geometrically fit inside the two of the β-CD cavities, forming $Au_{38}S_2(SAdm)_{20} \cap (\beta\text{-CD})_2$ conjugate by restricting the conjugation of other adamantane ligands due to the steric hindrance (Fig. 8). β-CD–adamantane conjugate improved the stability of the NCs even in harsh environments (highly oxidative or reductive environment) by blocking their charge transfer. These host–guest systems possess immense potential as building blocks in biomedical applications, such as drug delivery system and self-healing materials.

3.3.2. Covalent conjugation. Though Au NCs are ultrasmall in size and could be passively accumulated inside the tumor site through the EPR effect (passive targeting), active targeting of NCs is found to possess higher cellular internalization.[160] Many targeting molecules, such as folic acid,[161] cell penetrating peptides,[162] antibodies,[53] and aptamers,[163] have been successfully conjugated to Au NCs to specifically bind to receptors or binding moieties on the targeted sites. The most common chemical conjugation protocol is carbodiimide coupling, using 1-(3-dimethylaminopropyl)-3-ethylcarbodiimmide (EDC) hydrochloride as a crosslinker. Activation of carboxyl moieties using EDC and then coupling with amine-containing molecules leads to the formation of strong amide bonds. Besides the targeting moiety, drugs,[164] fluorescent dyes,[165] and computed tomography (CT) contrast agents,[166] can also be conjugated onto Au NC surface for its better functionality. For instance, Ding *et al.* have covalently conjugated a chemotherapeutic agent, thiolated doxorubicin (DOX-SH) and a tumor homing peptide (cyclic arginine–glycine–aspartate (cRGD)) onto the surface of BSA-protected Au NCs, and the resulting DOX/RGD-BSA-Au NCs nanocomposites were used as nanocarriers.[167] First, the covalent conjugation between cRGD and BSA-protected Au NCs was achieved through EDC coupling to target αvβ3 integrin receptors overexpressed on the cancer cells.[168,169] Then, to further conjugate DOX-SH to RGD-BSA-Au NCs, a water-soluble hetero-bifunctional crosslinker *N*-succinimidyl-3-(2-pyridyldithio) propionate (SPDP) was used to couple sulfhydryl moiety of DOX-SH and amine groups of BSA. The formation of irreversible bonds through covalent conjugation improved the stability of chemotherapeutic drugs in the complex biological media. Thus, bio-conjugation of Au NCs possesses immense potential in overcoming biological barriers to finally meet its desired functionalities.

4. Biomedical applications of surface-engineered Au NCs

Surface-engineered Au NCs have gained increasing interests among scientific communities due to their improved physicochemical and physiological properties, such as high stability in biological media, good biocompatibility, strong PL, and low toxicity. In this section, we highlight some applications of these surface-engineered Au NCs in several important biomedical sectors.

4.1. Intracellular biosensing and bioimaging

Imaging dynamic processes at cellular, sub-cellular and molecular level in real-time enables early detection and treatment of deadly diseases like cancer.[170,171] Fluorescence imaging (FI) is getting an immense attention in recent years due to the development of high quality fluorescent probes.[172,173] Semiconductor quantum dots have played a leading role as bioimaging probe but they suffer from inherent cytotoxicity.[174] As noble metal NCs possess good biocompatibility with good photo-stability, strong luminescence with microsecond luminescence lifetime, large Stokes shift (>200 nm), and near-infra red (NIR) emission, they are a promising class of luminescent materials for bio-related applications. For example, self-quenched BSA-protected Au NCs (Sq-Au NCs) (luminescence quenched due to the incorporation of disulphide bonds using dithiobis(succinimidyl propionate) (DSP) to aggregate BSA-Au NCs) were used for intracellular imaging of GSH.[175] An abnormal level of GSH (usually between 2–10 mM range)

serves as a biomarker for early stage detection of cancer. Upon treatment with millimolar concentration of GSH, the fluorescence of Sq-Au NCs was turned-on by the cleavage of the disulphide bonds using GSH, in a time and concentration dependent manner. When four kinds of cells namely, HepG-2, MCF-7, SCC-7, and Balb/3T3, were incubated with 0.2 mM Sq-AuNCs, the intracellular GSH concentrations were detectable with limits of detection of 1.00 ± 0.07, 1.10 ± 0.09, 1.43 ± 0.10, and 0.25 ± 0.01 mM, respectively.[175] Other ligand-protected Au NCs, such as 4,6-diamino-2-mercaptopyrimidine (DAMP)-protected Au NCs, have also been used to selectively detect GSH intracellularly.[176] Another important parameter that dictates the physiological state of the cell is temperature. Cancer cells possess higher intracellular temperature compared to normal cells due to their higher rates in metabolism.[177,178] In this context, a thermo-responsive green-emitting 6-aza-2-thiothymine (ATT)/arginine (Arg)-stabilized Au NC (ATT/Arg-Au NC) was used to probe the intracellular temperature of osteosarcoma MG-63 cells.[179] Both PL intensity and lifetime decreased gradually as temperature increased from 15 to 50 °C without any shift in their emission maxima. Significant increase in non-radiative recombination rate, k_{nr} (calculated using the equation $k_{nr} = (1 - QY)/\tau$, where τ is average lifetime) of ATT/Arg-Au NCs with negligible change in their radiation recombination rate, k_r ($k_r = QY/\tau$) was observed as temperature increased. Additionally, this Au NCs-based intracellular nano-thermometer has shown reversibility without observable hysteresis in several cycles of heating and cooling, highlighting its thermal- and photo-stability in the complex biological environment.

In addition to higher intracellular GSH concentration and temperature, cancer cells are also marked with specific antigens overexpressed on their membranes. Recently, a self-assembly based signal amplification strategy for specific detection and imaging of cancer cells was demonstrated.[153] Jiang *et al.* have synthesized dual-ligand-protected Au NCs, which were further modified with streptavidin (SA) and biotin moieties to form Au NC-SA and Au NC-biotin. When Au NC-SA and Au NC-biotin were incubated with biotinylated antibody labelled MCF-7 breast cancer cell line, controlled agglomeration of Au NCs on the surface of cancer cell membrane was observed (Fig. 9a). Through supramolecular interactions of SA-biotin moieties, intense green emission with high signal-to-noise ratio was seen mostly on the surface of the membrane. By utilizing the large two-photon absorption (TPA) and long PL lifetime of Au NC-SA and Au NC-biotin, multi-modal images of MCF-7 cells were reported with minimized auto-fluorescence and better spatial resolution (Fig. 9b).

Though PL imaging is a non-invasive and powerful tool, it might be difficult to generate the detailed anatomical information solely through PL. By combining with other macroscopic

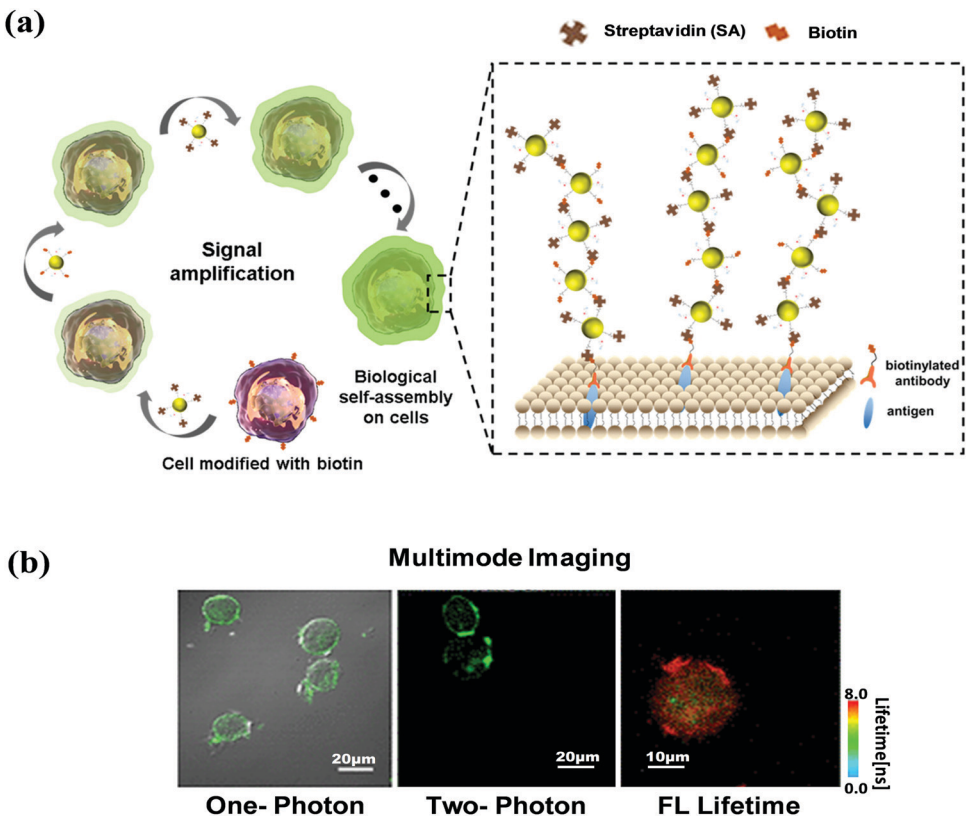

Fig. 9 (a) Schematic illustration of biological assembly process of surface-engineered Au NCs (Au NC-SA and Au NC-biotin) with biotinylated cancer cells. (b) One-photon, two-photon and fluorescence lifetime images of biotinylated MCF-7 cells assembled with (Au NC-SA/Au NC-biotin)$_2$/Au NC-SA. Reproduced with permission.[153] Copyright 2019, American Chemical Society.

imaging modalities such as computed tomography (CT), magnetic resonance imaging (MRI), and photoacoustic imaging (PAI), the utility of optical imaging data can be greatly improved. CT is the most used diagnostic tool due to its low cost and good spatial resolution. Au NCs possess inherent characteristics of good CT contrast agent due to the high X-ray attenuation coefficient and large atomic number (Z = 79) of Au atoms. Thus, Au NCs acting as dual-modal imaging probe (PL and CT) was demonstrated by Wu *et al.*[143] Orange-emitting Au NCs from the confocal laser scanning microscopy (CLSM) images revealed the intracellular accumulation of Au nanocomposites (aggregated Au NCs encapsulated into polyacrylic acid/mesoporous silica shell). On the other hand, animal studies manifested good CT contrast with better signal-to-noise ratio.[143] MRI has been utilized to improve spatial resolution in deep seated tumor. In addition to CT and MRI, PAI can also be combined to analyze the pathophysiological status of tumor such as micro-vessel density and oxygen saturation status. For example, Liu *et al.* have synthesized stimuli-responsive Au NCs decorated porous manganese monoxide nanocomposites (MnO@Au) for trimodal imaging of tumor-bearing mice.[180] In response to acidic pH within tumor microenvironment, Mn^{2+} ions were dissociated from the nanocomposites and diffused randomly inside the tumor (Fig. 10a). As Mn^{2+} ions are good MRI contrast agents, the interior of tumor was imaged and analyzed using T_1-weighted MRI image (T_1-weighted image is a pulse sequence in MRI, based on short repetition time (TR) and echo time (TE) of radiofrequency (RF) pulses). Contrast and brightness of T_1-weighted image depends on T_1 relaxation time of tissues, where short T_1 appears bright and long T_1 appears dark. Here, Mn^{2+} ions shorten the T_1 relaxation time of the tissues, thereby enhancing the contrast of the T_1-weighted image. The presence of Au NCs in the outer layer of MnO nanocomposites delays the release process of Mn^{2+} ions, thereby widening the diagnostic time frame. The delay in the T_1-weighted MRI image of MnO@Au is obvious by the appearance of bright signal at 24 h (Fig. 10b). Additionally, as Au NCs are good CT contrast agents, significantly enhanced Hounsfield scale (HU) values (depict the grayscale in CT imaging with values from −1000 to +3071 HU based on X-ray attenuation coefficient of tissues) were observed on the tumor site with detailed anatomical information (Fig. 10a). The efficient NIR absorption of MnO@Au nanocomposites enhanced the photoacoustic imaging depth for visualizing tumor microvasculature (Fig. 10c).[180] Within 2 hours post-intratumoral injection of MnO@Au nanocomposites, a strong photoacoustic signal intensity was observed with 1.8-fold higher than that of the PBS-treated sample, illustrating the effectiveness of MnO@Au nanocomposites in multimodal imaging.

Recently, fluorescence imaging depth of Au NCs were significantly improved by tuning the PL to NIR-II/shortwave infrared (SWIR) window of 900–1700 nm.[181,182] The emission of atomically precise Au_{25} NCs centered at 1120 nm has allowed the long wavelength photon to cross the biological barrier and penetrate the deep biological tissues, remarkably improving the spatial resolution. By combining with dynamic imaging modalities, precise location of impaired blood vessels in brain tissue of the mice were identified. Additionally, real-time monitoring of cancer metastasis was performed by Au_{25} NCs mediated NIR-II imaging. Higher uptake of Au_{25} NCs in tumor induced region of the mice was observed in less than 30 s. After 5 min of injection, the primary tumor and metastatic region were clearly seen with significant uptake of Au_{25} NCs (~10.5 times higher than that of the normal tissues). Principal component analysis (PCA) was found to be useful in analyzing the time course imaging data, which can clearly distinguish between the primary tumor, blood vessel, and metastatic region.[182]

4.2. Theranostic applications

4.2.1. Chemotherapy. The treatment strategies for many diseases (*e.g.*, cancer) highly depend on the extent of the disease (staging) and the clinical state of the patients. The well-designed

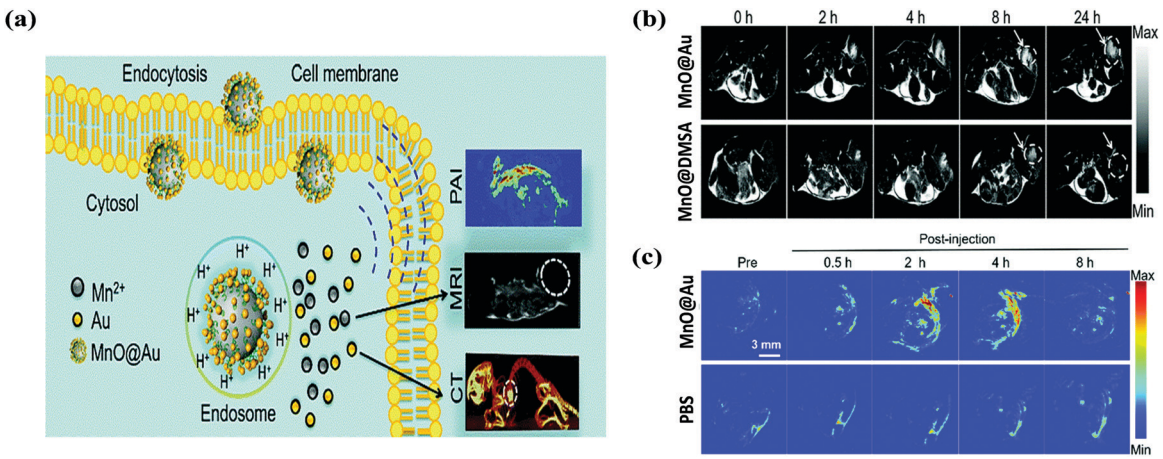

Fig. 10 (a) Schematic illustration of endocytosis of MnO@Au nanocomposites and their pH responsive MR/CT/PA imaging applications. (b) Time dependent T_1-weighted MRI images of tumor-bearing mice after intratumoral injection of 50 μL of 2 mg mL^{-1} MnO@Au (upper row) and MnO@DMSA (lower row). (c) The *in vivo* PAI image of tumor-bearing mice after intratumoral injection of 200 μL of 2 mg mL^{-1} MnO@Au (upper row) and PBS (lower row). Reproduced with permission.[180] Copyright 2018, The Royal Society of Chemistry.

Au NC probes discussed above help in the staging of the disease. In this context, Au NCs-based sub-cellular targeted therapy of cancer is highly feasible. Mitochondrial targeting of nanomaterials has become a hot area of research in cancer theranostics due to its capability in controlling the programmed cell death termed "apoptosis".[183] Recently, by changing the ligands on the surface of Au NCs, specific mitochondrial targeting was achieved. For example, Yang *et al.* have tuned the fate of Au NCs intracellularly by replacing GSH ligand with (4-mercaptobutyl)triphenyl phosphonium bromide (MTPB) on $Au_{18}(SG)_{14}$ NCs through a ligand exchange method.[184] The MTPB-substituted Au_{18} NCs showed higher accumulation into mitochondria, while the unmodified $Au_{18}(SG)_{14}$ NCs preferably accumulated in lysosomes. Anti-tumor effect of Au NCs has also been tuned based on its preferential intracellular localization. For instance, Zhai *et al.* have synthesized two types of peptide-protected Au NCs namely, $Au_5Peptide_3$ and $Au_{22}Peptide_{10}$, and tested on epidermal growth factor receptor (EGFR)-positive nasopharyngeal carcinoma cell line (CNE1) and EGFR-negative breast cancer cell line MCF-7.[185] The peptide used here is H_2N-YHWYGYTPQNVI-KKKKYCC-COOH, where YHWYGYTPQNVI serves as EGFR targeting sequence, and YCC is designed for the capture of gold ions, while KKKK is to increase the stability of the peptide. $Au_5Peptide_3$ showed ~50% cell death on EGFR-positive CNE1 cell line in 24 h and almost completed eradication in 48 h (treated with Au atom concentration of 80 μM). $Au_{22}Peptide_{10}$, on the other hand, showed no killing effect regardless of EGFR-positive or -negative cell lines. When the targeting peptide is replaced by BSA on the surface of Au_5 NCs, no cytotoxicity was observed. This data highlights the need for targeting moiety on the surface of Au_5 NCs to enable cellular penetration and its corresponding cytotoxic activity. Structured illumination microscopy (SIM) and TEM images (Fig. 11a and b) illustrate the presence of $Au_5Peptide_3$NCs in mitochondria, thereby showing selective apoptosis of Au_5 NCs over Au_{22} NCs (accumulated in lysosomes) through the mitochondria dependent pathway. Upregulation of pro-apoptotic protein and downregulation of anti-apoptotic protein were observed in a concentration dependent manner of Au_5 NCs (0–80 μM). Dose dependent *in vivo* anti-tumor effect of $Au_5Peptide_3$ NCs and free peptide on CNE1 tumor xenograft model of nude mice are shown in Fig. 11c. The change in tumor volume in $Au_5Peptide_3$ treated mice is seen in time and dose dependent manner. After 10 days of treatment, lower dose of $Au_5Peptide_3$ could not suppress the tumor growth.[185] This may be due to the rapid renal clearance of Au NCs.

4.2.2. Photodynamic therapy (PDT). Photodynamic therapy involves the use of photosensitizers as a therapeutic molecule that gets activated by appropriate wavelength of light and produces reactive oxygen species (ROS) in the presence of oxygen. Various ROS species, such as singlet oxygen ($^1O_2$), superoxide (O_2^-), peroxide (H_2O_2), and hydroxyl radical (OH^-), can cause localized oxidative damage to DNA and other macromolecules when photosensitizers were taken intracellularly.[186] Photosensitizers are usually non-toxic molecules but when they were triggered by a specific wavelength of light, the valence electrons would jump from the ground state to the singlet excited state, which then undergo an intersystem crossing to a long lived triplet excited state. ROS can be generated either through the electron transfer from long lived triplet excited state of photosensitizers to molecular oxygen (type I reaction pathway) or through the energy transfer to triplet state of oxygen (type II reaction pathway).[187] PDT is mainly targeting at the tumor sites where surgery is not possible.[188]

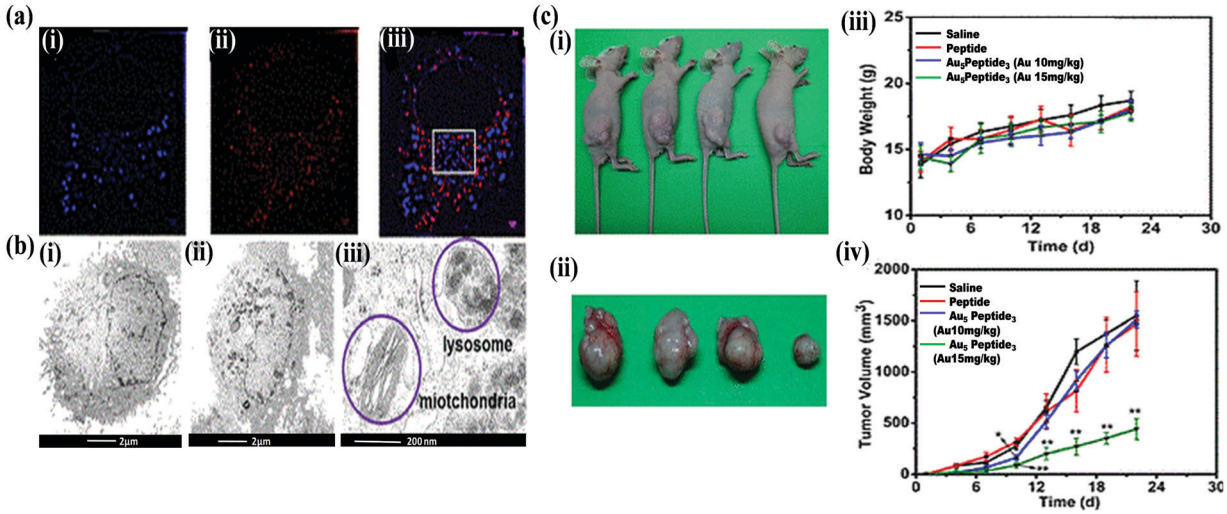

Fig. 11 (a) The structured-illumination high resolution images of CNE1 cells: (i) treated with $Au_5Peptide_3$ (80 μM Au, 24 h), (ii) followed by mitotracker stained image, and (iii) the merged image. (b) TEM images of CNE1 cells: (i) treated with $Au_5Peptide_3$ at 80 μM Au for 24 h, (ii) control cells, and (iii) the higher magnification image of $Au_5Peptide_3$ treated cells. (c) (i) The *in vivo* antitumor effect of $Au_5Peptide_3$ NCs and free peptide on CNE1 tumor bearing nude mice, (ii) their corresponding tumors removed from the mice of four different groups (from left to right: saline group, free peptide of 110 mg kg^{-1} treated group, $Au_5Peptide_3$ of serial dosage of 10 mg kg^{-1} and 15 mg kg^{-1} treated groups), (iii) the average body weight, and (iv) average tumor volume of four groups of nude mice taken at different time points. Reproduced with permission.[185] Copyright 2018, American Chemical Society.

Ultrasmall Au NCs possess unique photo-physical properties, such as large two-photon absorption cross section, NIR emission, long lived triplet states, and good QYs, which can be used to construct photosensitizers for PDT.[189] Several Au NCs, such as captopril-protected Au_{25} NCs, have been used to produce singlet oxygen ($^1O_2$) species under visible/NIR irradiation.[190,191] The photochemical reactivity of Au NCs was analyzed by Sakamoto *et al.*, where different sized Au NCs embedded in a polymer film showed different performance in the presence of oxygen and light.[192] Single molecule fluorescence spectroscopy study revealed that spin multiplicity of excited state (either singlet or triplet state) of Au NCs plays a major role in their photochemistry.[192] Recently, these findings were substantiated by thorough analysis of three different metal NCs namely, GSH-protected Au_{25} and Ag_{32} NCs and hexane-thiol-protected Au_{144} NCs, for their $^1O_2$ generation efficiency.[193] Au_{144} showed two times higher in magnitude of $^1O_2$ generation compared to the other two NCs, and they were several orders of magnitude higher than those generated by larger NPs. The high efficiency $^1O_2$ generation of Au_{144} NCs is due to its high absorption cross-section to volume ratio with increased triplet excited state populations (Fig. 12a). The ligands on Au_{144} NCs can be another reason for its enhanced $^1O_2$ generation compared to Au_{25} and Ag_{32}. Moreover, PDT of Au NCs was explored by using GSH-protected Au_{25} NCs due to its good water solubility. Two-photon excitation (800 nm laser source) of Au_{25} NCs treated mouse fibroblast cells showed cell necrosis in less than 15 minutes (Fig. 12b).[193]

Some recent studies also demonstrated that Au NCs can improve the singlet oxygen generation capability of organic photosensitizers. For example, lipoic acid-protected Au_{18} NCs can be conjugated with protoporphyrin IX (PPIX) (denotes as PFL-Au NCs), which showed an improved $^1O_2$ yield ($\sim$80%) compared to the PPIX alone ($\sim$63%) upon laser irradiation at 530 nm. It was suggested that the enhanced charge transfer between Au NCs and PPIX is the reason for improved singlet $^1O_2$ generation of PFL-Au NCs.[194] Since these Au NCs showed fast renal clearance, they are often co-assembled with polymers or other molecules. The self-assembly of ultrasmall GSH-Au NCs with protamine and hyaluronic acid polymers, increased the blood circulation time, as well as improved the PL QYs and the singlet oxygen generation of Au NCs.[195]

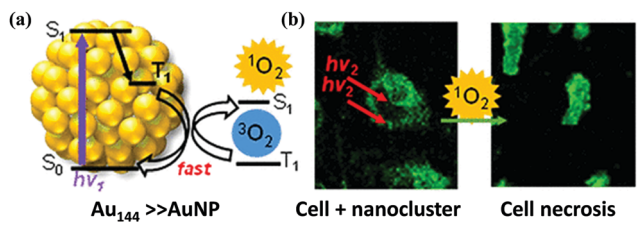

Fig. 12 (a) Schematic illustration of higher $^1O_2$ generation of Au_{144} NCs compared to Au NPs, (b) two-photon excited fluorescence microscopy image of mouse fibroblast cell treated with 400 mg mL^{-1} of GSH-protected Au_{25} NCs. Reproduced with permission.[193] Copyright 2017, American Chemical Society.

For *in vivo* PDT applications, near-infrared II (NIR-II) light is recommended in order to avoid absorption and autofluorescence by tissue. NIR-II light activated PDT of Au NCs was recently demonstrated *in vivo* by Chen *et al.*[196] Human serum albumin (HSA)- and catalase-protected Au NCs (Au NCs@HSA/CAT) can convert tumor endogenous hydrogen peroxide (H_2O_2) to oxygen. Under NIR-II light irradiation, the *in situ* generated oxygen was converted to singlet oxygen by Au NCs, which in turn helped to eradicate the tumor (Fig. 13a). While the *in vitro* singlet oxygen generation efficiency of Au NCs@HSA/CAT under 1064 nm irradiation was lower than the organic photosensitizer – chlorin e6 (Ce6), their capability of producing singlet oxygen in deep tumor was appreciable (Fig. 13b). It was evident that after covering Ce6 with 3 mm and 10 mm thick pork tissues, their efficiency was significantly reduced. Whereas at a similar condition, Au NCs can still produce singlet $^1O_2$ and thus eradicated the targeted cells efficiently. Deeper tissue penetration of NIR-II light and subsequent photosensitization of Au NC nanocomposite can explain its superior killing efficacy.

PDT destroys cancer cells and damages associated molecular patterns (DAMP) behind, which in turn triggers host immune response to selectively uptake those DAMPs.[197] As majority of tumors would develop immune-suppressive environment, combinatorial therapy of PDT with chemo-immunotherapy can eradicate malignant cells by preventing further metastasis. Recently, Yu *et al.* have combined immune checkpoint inhibitor with photosensitizers and chemotherapeutic drug – paclitaxel, to trigger immune response and exert anti-tumor effect.[198]

4.2.3. Radiotherapy (RT). More than 50% of cancer patients receive either radiotherapy (RT) alone or combined chemo-radiotherapy.[199] RT involves the use of high energy ionizing radiations to impart its biological effects on tumor cells.[200] Though RT is efficient in tumor eradication, there are several challenges to overcome. They are: (1) damage to the healthy cells during the treatment process; (2) hypoxic nature of tumor microenvironment (TME), leading to insignificant ROS production; and (3) higher intracellular anti-oxidant (*e.g.*, GSH) concentration that neutralizes the effect of free radicals, and the combined effects of which have rendered tumor cells radioresistant.[201,202] A number of nanomaterials have been used to overcome the above limitations. Due to the high atomic number of gold (Z = 79), Au NPs were studied for decades as an efficient radiosensitizer. Au NPs exhibited strong adsorption, scattering and re-emitting capability of radiation, which is effective in locally increasing the radiation effects.[9] All these unique features can facilitate the translation of Au NPs from bench to clinical trials. However, the poor clearance efficacy of Au NPs from the body represents a major obstacle for their clinical applications. To circumvent this issue, the ultrasmall Au NCs have emerged as a promising class of radiosensitizers with good pharmacokinetic properties.[8,203,204] Recently, atomically precise alkynyl(levonorgestrel)-protected Au_8 NCs showed good radiosensitizing effects, leading to irreversible apoptosis of tumor cells. Au_8 NCs with an X-ray dose of 4 Gray (Gy) showed significant tumor inhibition ratio of 74.2% (due to localized

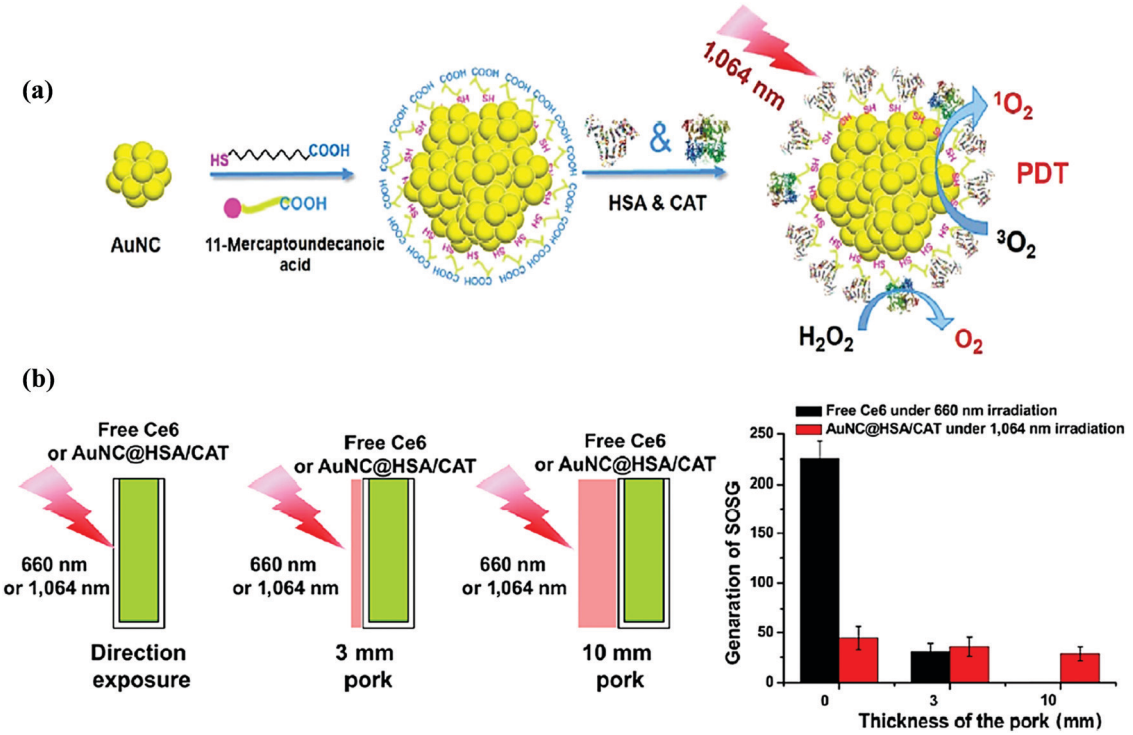

Fig. 13 (a) Schematic illustration of the synthesis of Au NC@HSA/CAT nanocomposites and its $^1O_2$ generation under NIR-II light irradiation. (b) Schematic illustration of the experimental design, where samples were blocked by pork slices of varied thicknesses (0, 3, and 10 mm thick pork slices) and irradiated by 660 and 1064 nm laser source with the same power density. Reproduced with Permission.[196] Copyright 2018, Springer Nature.

production of ROS by Au NCs) compared to tumors irradiated with X-ray alone.[10] The choice of surface ligands plays an important role in exerting Au NCs radio sensitivity. In this context, the radiotherapeutic potential of arginine-modified glutathione-protected Au NCs (GSH-2Arg-Au NCs) and GSH-passivated Au NCs (GSH-Au NCs) was compared on U87MG human glioblastoma 3D spheroid model.[205] It was observed that though GSH-2Arg-Au NCs has shown 4-fold increase in spheroid uptake when compared to GSH-Au NCs, the radiosensitization of GSH-2Arg-Au NCs on decreasing the spheroid viability was lower than that of GSH-Au NCs treated sample. The plausible reason for such passivating effects on radiotherapeutic activity might be the formation of extracellular aggregates of GSH-2Arg-Au NCs when compared to homogenous distribution of GSH-Au NCs throughout the micro tumors.

Targeting capacity of radiosensitizers is an important consideration to selectively impart its efficacy to the tumor specific region. Recently, Au_{25} NCs were designed as radiosensitizers specifically for targeting the prostate cancer cells.[206] Custom-designed peptide-tagged prostate specific membrane antigen targeting ligand (CY-PSMA-1, here CY denotes cysteine and tyrosine) protected Au_{25} NCs (CY-PSMA-1-Au_{25} NCs) were synthesized for targeting PSMA receptor positive cancer cells (PC3pip). As a control study, a PSMA receptor negative cell line (PC3flu) was used. Gold content in each set of cells was analyzed using ion coupled plasma mass spectrometry (ICP-MS), which suggests that PC3pip cells had almost a two-fold higher Au content than that of PC3flu cells. Due to such high Au content, the ROS production in PC3pip cells upon irradiation was ~3.3 times more than that of PC3flu cells, indicating the role of cell-specific internalization of Au NCs. Additionally, these CY-PSMA-1-Au_{25} NCs were cleared rapidly from the body within 3 h post injection.

Another serious issue faced by radiotherapeutics for decades is radio-resistance. Radio-resistance is mainly caused by oxygen depletion and higher GSH intracellular concentration.[202] To address this challenge, a recent study designed BSA-Au-MnO_2 nanocomposite using the biomineralization approach, where MnO_2 served as a catalyst for converting tumor endogenous H_2O_2 to oxygen.[207] Au NCs on the other hand, acted as radiosensitizers by absorbing and depositing X-ray energy within tumors to enhance radiotherapy. The acidic tumor micro-environment triggered dissociation of MnO_2 from the nanocomposite, thereby releasing ultrasmall BSA-Au NCs within tumor (Fig. 14a). Intra-tumor penetration of these NCs can enhance the radio therapeutic performance, as shown in Fig. 14b and c. Tumor growth curves of transplantable tumor 4T1 bearing mice were divided into 6 groups based on the treatment they received. BSA-Au-MnO_2 nanocomposite with 6Gy radiation has reduced the tumor volume many folds than that of the untreated group or radiation alone group.[207] This data highlights the importance of developing multifunctional composites with Au NCs as one of the key components to tackle some of the existing problems in cancer radiotherapy.

4.3. Antibacterial application

Antibiotic resistant bacterial infections are now becoming a worldwide threat.[208] Use of nanomaterials as an alternative to

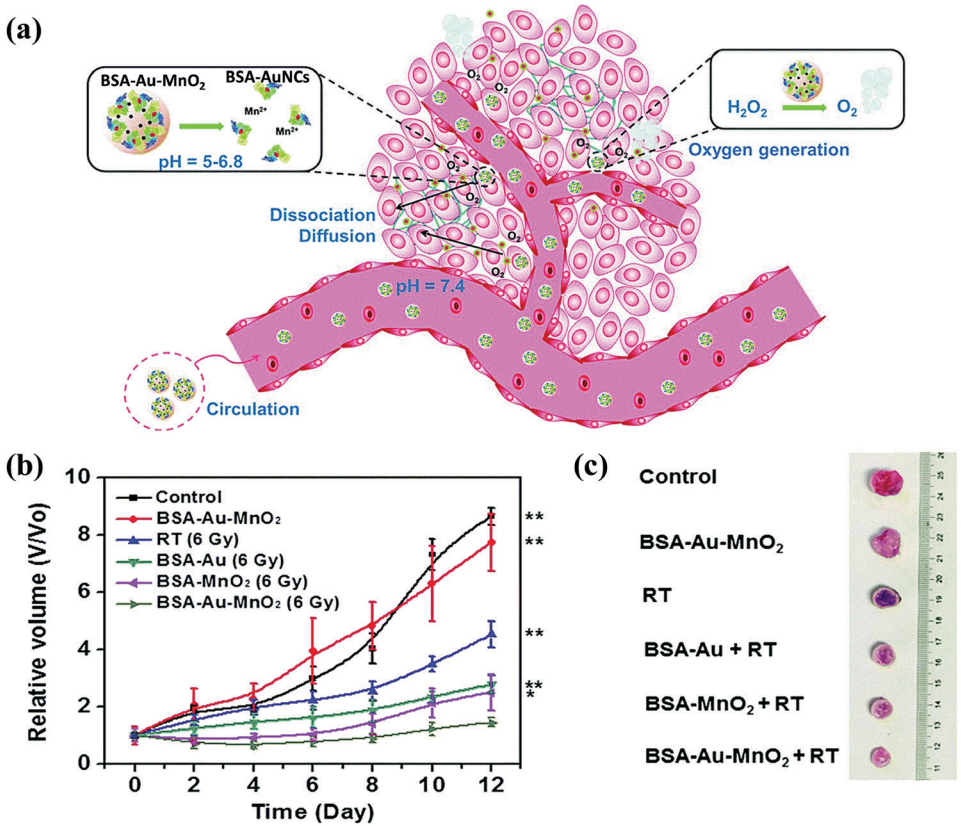

Fig. 14 (a) Schematic illustration of tumor responsive degradation of larger BSA-Au-MnO_2 NPs to smaller ones allowing hypoxia relief and intra-tumor penetration. (b) Tumor growth curves of 6 groups of transplantable tumor cell line (4T1) bearing mice consists of untreated control, intravenously injected BSA-Au-MnO_2 treated group, x-radiation (6Gy) alone, intravenously injected BSA-Au or BSA-MnO_2 or BSA-Au-MnO_2 with radiation (6Gy) treated groups. (c) Photographs of corresponding tumors after 12 days of treatment of all 6 groups. Reproduced with permission.[207] Copyright 2017, Royal Society of Chemistry.

conventional antibiotics has received increasing attention due to the wide-spectrum antimicrobial action of various NPs. Since antibacterial mechanism of NPs is not specific, the probability of bacterial resistance is lower than the conventional antibiotics.[209] Among various NPs, silver NPs have been studied the most. The effects of size, shape, surface coating of Ag NPs on their antimicrobial efficacy were analyzed in detail.[210–212] The application of Ag NCs in antibacterial therapy is an important area of research. On the other hand, though Au NCs were being used in radiotherapy, PDT or other biomedical applications, the inherent antibacterial Au NCs were rarely reported. Recently, our group explored the antibacterial potential of MHA-protected Au_{25} NCs on both Gram-positive and Gram-negative strains.[13] In particular, Au NCs can suppress more than 90% of Gram-positive *Staphylococcus aureus* strains with slightly lower killing efficacy on Gram-negative *Pseudomonas aeruginosa* after 2 hours of treatment. This difference may be due to the bulky cell membrane envelope in Gram-negative bacteria compared to Gram-positive ones. Our group also explored the antibacterial potential of large sized MHA-protected Au NPs to understand the core-size effect on bacterial strains. It was observed that even with ~15-fold increase in Au NP concentration with respect to Au_{25} NCs, only 8% killing efficacy on *S. aureus* strains was achieved. In a more recent study, we have also studied the effect of surface charges of ultrasmall Au NCs on their antibacterial efficacy.[213] SYTOX green nucleic acid staining dye, which is a cell membrane impermeant dye able to enter into dead cells with ruptured membrane, was used to differentiate between live and dead bacteria. From fluorescence images, higher antibacterial potential was observed with negatively charged Au NCs compared to positively/neutrally charged Au NCs (Fig. 15a). It is also interesting to note that though cysteine (Cys)-protected Au_{25} NCs had higher internalization into the bacterial cells, they possessed lower killing efficacy compared to MHA-protected Au_{25} NCs. A higher amount of ROS was generated by MHA-protected Au_{25} NCs, which contributes to its higher antibacterial potential.

Recently, the effect of Au NCs on superbugs has been studied *in vivo*. For example, Xie *et al.* have synthesized a series of cationic Au NCs and tested their efficacy on wide range of Gram-positive multi-drug resistant bacteria.[214] Among them, quaternary ammonium (QA)-modified Au NCs (QA-Au NCs) were found to possess lower minimum inhibitory concentration (MIC) on methicillin-resistant *S. aureus* (MRSA) and vancomycin resistant *Enterococci* (VRE) strains compared to other cationic Au NCs. The mechanisms of interaction of QA-Au NCs on *S. aureus* as model bacteria were studied using

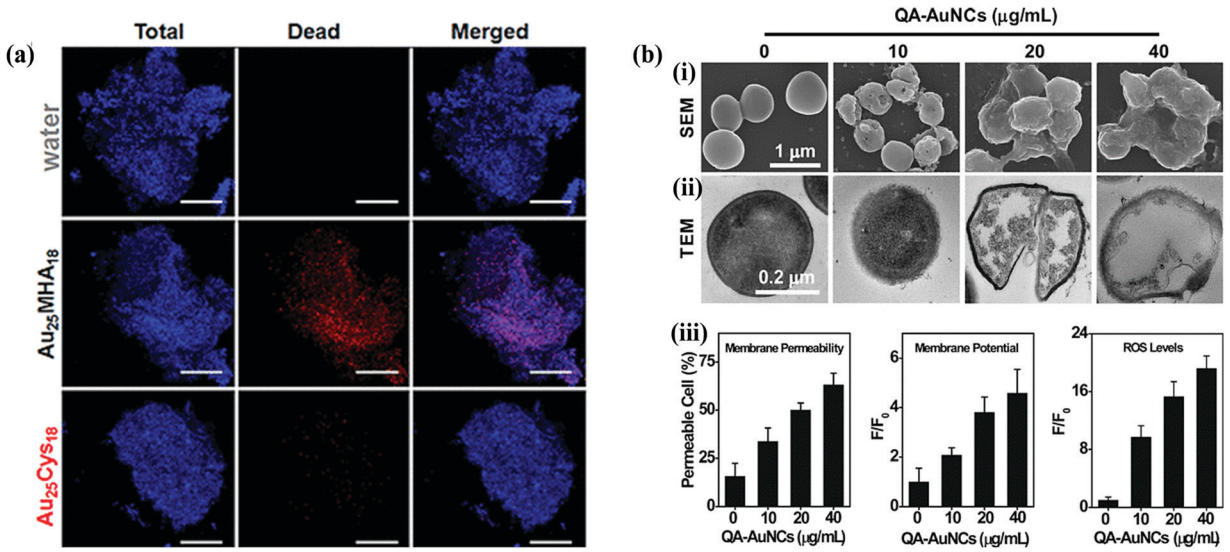

Fig. 15 (a) Fluorescence images of *S. aureus* bacterial spheroids after 2 h treatment with water, MHA-protected and Cys-protected Au_{25} NCs. Dead channel showed the antibacterial potential of Au_{25} NCs. Here, SYTOX green dye stained dead cells (false colour: red) and total cells were stained using Hoechst 33342 dye. Scale bar is 100 μm. Reproduced with permission.[213] Copyright 2018, American Chemical Society. (b) Morphological changes of *S. aureus* after treated with various concentrations of QA-Au NCs, observed in (i) SEM and (ii) TEM images (iii) the graphical representation of changes in membrane permeability, membrane potential and ROS generation of QA-Au NCs treated *S. aureus* bacterial model. Reproduced with permission.[214] Copyright 2018, Wiley-VCH.

scanning electron microscopy (SEM) and transmission electron microscopy (TEM). As the concentration of QA-Au NCs increased, membrane rupture was observed with increased membrane permeability and higher generation of ROS (Fig. 15b).

Stimuli-responsive drug delivery system not only reduces damage to host cells but also prevents antibiotic resistance. Recently, Pranantyo *et al.* have synthesized smart pH sensitive citraconyl-protected antimicrobial peptide (AMP), and used this AMP to protect Au NCs to construct a drug carrier.[215] The bacterial infection site was marked with localized acidosis due to the host inflammatory responses and bacterial metabolism. In particular, the acidic pH cleaved the citraconyl moieties exposing the cationic AMP-modified Au NCs to the bacterial infection site. These NCs showed higher antibacterial activity with MIC of 4–16 μg mL^{-1} toward both Gram-positive and Gram-negative bacteria compared to free peptides (MIC of 8–64 μg mL^{-1}). In addition to the internal stimuli, the external stimuli were also enabled to eradicate the bacterial infection. Antimicrobial photodynamic therapy (aPDT) was found to be a non-invasive and attractive therapeutic modality in post-antibiotic era.[216] aPDT with targeting capability were integrated with imaging modality forming multifunctional Au NCs against MRSA. Red-emitting BSA-Au NCs were surface modified with anti-staphylococcal antibodies (IgG) and loaded with photosensitizers (PS) to specifically target and eradicate MRSA. Based on the irradiation time, varying degree of antibacterial efficacy against MRSA was observed with higher killing percentage for BSA-Au-IgG–PS complexes, compared to that with free photosensitizers alone.[217]

For *in vivo* studies, to avoid fast renal clearance of these ultrasmall NCs and to improve its functionality, an antimicrobial formulation composed of holmium–graphene oxide–Au NCs (Ho–GO–Au) nanocomposite has been recently synthesized.[218] The sharp edges of graphene oxide (GO) nanosheets can pierce the bacterial membrane and generate ROS intracellularly. Complexation of holmium ions on the GO nanosheets controlled the orientation of nanosheets against bacterial membrane under weak magnetic field. The antibacterial effect of magnetically aligned Ho–GO–Au nanosheets are shown in Fig. 16. After 2 h treatment of *S. aureus* with GO–Au (without magnetic pre-alignment), Ho–GO and Ho–GO–Au under magnetic pre-alignment Ho–GO(+) and Ho–GO–Au(+), a higher degree of SYTOX green dye in the merged channels of Ho–GO–Au(+) with significant increase of ROS generation was observed, revealing the synergistic performance of Ho, GO, and Au NCs. On the aspect of pharmacokinetics and toxicology of Ho–GO–Au nanoconjugates, external magnetic field responsive GO with its bio-degradable components minimizes the toxicity during circulation. The IC50 value of Ho–GO–Au was found to be safe for normal human cell lines, paving the way for its potential *in vivo* application.[218]

5. Conclusion

The ultimate goal of interfacial engineering is to design multifunctional Au NCs for biomedical applications through in-depth understanding of the interface between NC surface and biological systems. As the size of Au NCs is extremely small, Au NCs can interact with the proteins, cells and intracellular components, in a distinctly different way from their larger counterparts, Au NPs. The surface properties of Au NCs also play a key role for their *in vivo* biomedical applications. The choice of suitable ligands as well as the proper balance between the surface charge and hydrophobicity is important to achieve

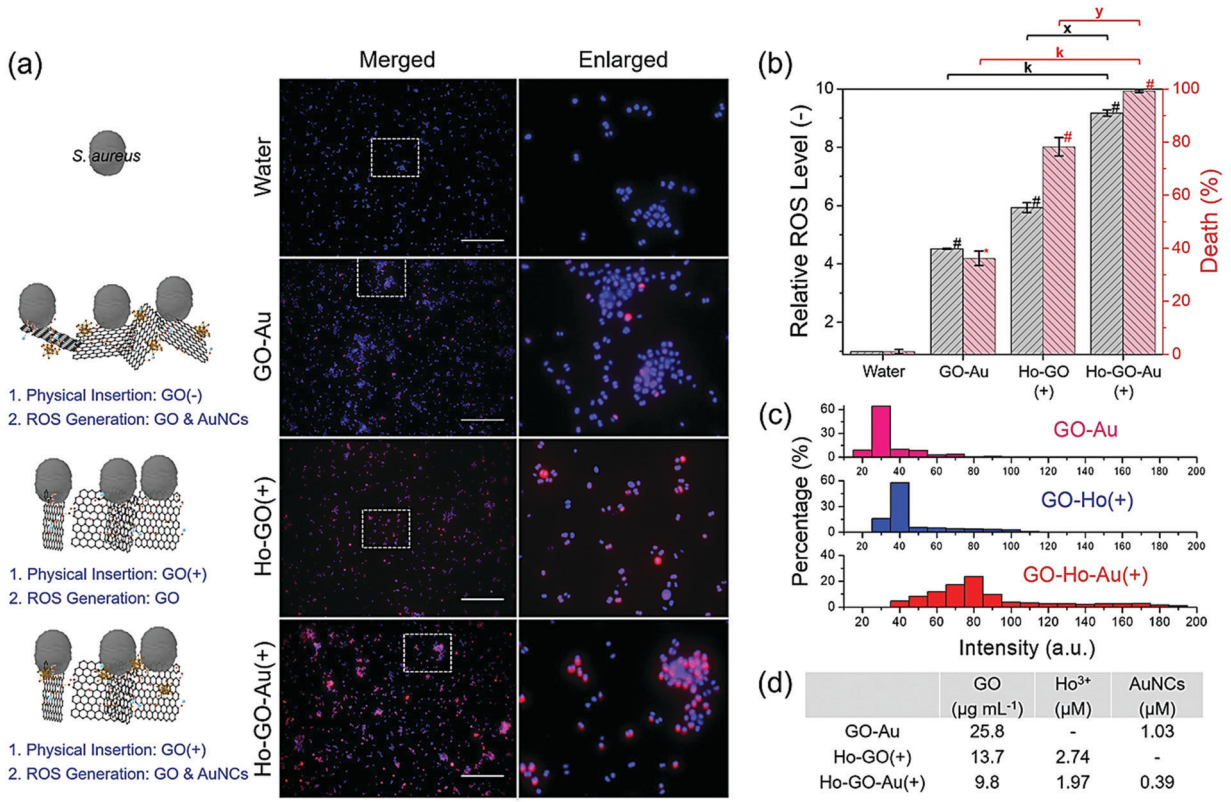

Fig. 16 Synergistic antimicrobial efficiency of magnetically aligned Ho–GO–Au nanocomposite. (a) Representative fluorescence images of the *S. aureus* after 2 h of treatment with GO–Au, Ho–GO under magnetic pre-alignment (Ho–GO(+)) and Ho–GO–Au under magnetic pre-alignment (Ho–GO–Au(+)). The dead cells were stained by SYTOX green dye (false colored into red), while total cells were stained by Hoechst 33342 (blue). Scale bars are 25 μm. (b) Relative intracellular ROS production level of *S. aureus* (grey columns) and death percentage of *S. aureus* (red column) after 2 h of treatments of various groups. Here 'k' represents significance of Ho–GO–Au(+) against GO–Au treated group, 'x' represents significance of Ho–GO–Au(+) against Ho–GO(+) treated group and 'y' represents significance of Ho–GO–Au(+) against Ho–GO(+) treated group. (c) Histogram of the SYTOX green intensity inside *S. aureus* cells after each treatment. (d) Half maximal inhibitory concentrations (IC50) of GO–Au, Ho–GO(+), and Ho–GO–Au(+). Reproduced with permission.[218] Copyright 2019, Wiley-VCH.

the desired performance. In this review article, we have highlighted that through proper interfacial engineering of Au NCs, better physicochemical and pharmacokinetic properties can be achieved. Once the desired features are confirmed, their unique properties can be applied for various applications. The promising biomedical applications of surface-engineered Au NCs include bioimaging, biosensing, PDT, RT, and antibacterial therapy.

Despite the recent advances on the understanding of nano-bio interfaces, a number of research gaps still persist in translation of these Au NCs from bench to clinics. So far, most of the studies rely on the EPR effect to achieve tumour uptake, and the efficiency of EPR for NCs uptake is a continuous concern. For better therapeutic outcome, active targeting strategies should be developed in future. Such strategies will help achieve better cellular internalization of Au NCs, which can greatly increase their acceptance in diverse sectors of biomedical applications. For instance, the conjugation of active photosensitizers with the targeting moieties on Au NCs might be effective against multi-drug-resistant bacteria and cancer cells due to its multiple killing mechanisms. Luminescent Au NCs could also be used as imaging probes for simultaneous diagnostics and therapy. Moreover, precisely personalized nanomedicine represents future direction of cancer treatment, as cancer appears heterogeneous not only from person to person but also within the person. In this scenario, more elaborate *in vitro* settings are needed to process the functionalized metal NCs before performing an *in vivo* analysis. Integration of microfluidics and *in vitro* three-dimensional (3D) culture models (*e.g.*, 3D spheroid model and heterotypic microtumor model) may help to closely mimic the *in vivo* tumor microenvironment. This may also be beneficial to understanding the spatiotemporal changes in cancer progression and cancer metabolism. We envisage that by combining the efforts of researchers from various fields, it would be possible to accelerate or advance the translation of surface-engineered Au NCs-based nanomedicine from bench to clinics.

Conflicts of interest

The authors declare no competing financial interest.

Acknowledgements

This work is financially supported by the Ministry of Education (MOE), Singapore, under Grants R-279-000-481-112 and

R-279-000-538-114. G. S. Yuvasri acknowledges the National University of Singapore for her research scholarship.

References

1 R. Jin, C. Zeng, C. M. Zhou and Y. Chen, *Chem. Rev.*, 2016, **116**, 10346–10413.
2 I. Chakraborty and T. Pradeep, *Chem. Rev.*, 2017, **117**, 8208–8271.
3 D. Cassano, S. Pocoví-Martínez and V. Voliani, *Bioconjugate Chem.*, 2018, **29**, 4–16.
4 X. Dou, X. Chen, H. Zhu, Y. Liu, D. Chen, X. Yuan, Q. Yao and J. Xie, *Dalton Trans.*, 2019, **48**, 10385–10392.
5 S. Palmal and N. R. Jana, *Wiley Interdiscip. Rev.: Nanomed. Nanobiotechnol.*, 2014, **6**, 102–110.
6 L. Y. Chen, C. W. Wang, Z. Yuan and H. T. Chang, *Anal. Chem.*, 2015, **87**, 216–229.
7 A. Cantelli, G. Battistelli, G. Guidetti, J. Manzi, M. Di Giosia and M. Montalti, *Dyes Pigm.*, 2016, **135**, 64–79.
8 T. Uptake, H. R. Clearance, X. Zhang, Z. Luo, J. Chen, S. Song, X. Yuan, X. Shen and H. Wang, *Sci. Rep.*, 2015, **5**, 8669.
9 N. Goswami, Z. Luo, X. Yuan, D. T. Leong and J. Xie, *Mater. Horiz.*, 2017, **4**, 817–831.
10 T. T. Jia, G. Yang, S. J. Mo, Z. Y. Wang, B. J. Li, W. Ma, Y. X. Guo, X. Chen, X. Zhao, J. Q. Liu and S. Q. Zang, *ACS Nano*, 2019, **13**, 8320–8328.
11 Y. S. Chen and P. V. Kamat, *J. Am. Chem. Soc.*, 2014, **136**, 6075–6082.
12 H. Choi, Y. S. Chen, K. G. Stamplecoskie and P. V. Kamat, *J. Phys. Chem. Lett.*, 2015, **6**, 217–223.
13 K. Zheng, M. I. Setyawati, D. T. Leong and J. Xie, *ACS Nano*, 2017, **11**, 6904–6910.
14 W. Chen, J. Lin, W. Chen, E. Wei-guang and Y. Chen, *Nanomedicine*, 2010, **5**, 755–764.
15 K. G. Stamplecoskie, Y. S. Chen and P. V. Kamat, *J. Phys. Chem. C*, 2014, **118**, 1370–1376.
16 I. Russier-Antoine, F. Bertorelle, M. Vojkovic, D. Rayane, E. Salmon, C. Jonin, P. Dugourd, R. Antoine and P. F. Brevet, *Nanoscale*, 2014, **6**, 13572–13578.
17 T. Higaki, C. Liu, M. Zhou, T. Y. Luo, N. L. Rosi and R. Jin, *J. Am. Chem. Soc.*, 2017, **139**, 9994–10001.
18 M. Agrachev, M. Ruzzi, A. Venzo and F. Maran, *Acc. Chem. Res.*, 2019, **52**, 44–52.
19 C. Zeng, T. Li, A. Das, N. L. Rosi and R. Jin, *J. Am. Chem. Soc.*, 2013, **135**, 10011–10013.
20 M. Farrag, M. Tschurl and U. Heiz, *Chem. Mater.*, 2013, **25**, 862–870.
21 H. Qian, M. Zhu, C. Gayathri, R. R. Gil and R. Jin, *ACS Nano*, 2011, **5**, 8935–8942.
22 H. Yu, B. Rao, W. Jiang, S. Yang and M. Zhu, *Coord. Chem. Rev.*, 2019, **378**, 595–617.
23 K. L. D. M. Weerawardene, E. B. Guidez and C. M. Aikens, *J. Phys. Chem. C*, 2017, **121**, 15416–15423.
24 L. Wu, W. Fang and X. Chen, *Phys. Chem. Chem. Phys.*, 2016, **18**, 17320–17325.
25 G. Li and R. Jin, *Acc. Chem. Res.*, 2013, **46**, 1749–1758.
26 X. Wan, J. Wang, Z. Nan and Q. Wang, *Sci. Adv.*, 2017, **3**, 1–7.
27 R. R. Nasaruddin, T. Chen, N. Yan and J. Xie, *Coord. Chem. Rev.*, 2018, **368**, 60–79.
28 M. Brust, M. Walker, D. Bethell, D. J. Schiffrin and R. Whyman, *J. Chem. Soc., Chem. Commun.*, 1994, 801–802.
29 M. Zhu, E. Lanni, N. Garg, M. E. Bier and R. Jin, *J. Am. Chem. Soc.*, 2008, **130**, 1138–1139.
30 R. Jin, *Nanoscale*, 2010, **2**, 343–362.
31 R. Jin, H. Qian, Z. Wu, Y. Zhu, M. Zhu, A. Mohanty and N. Garg, *J. Phys. Chem. Lett.*, 2010, **1**, 2903–2910.
32 Z. Wu, M. A. MacDonald, J. Chen, P. Zhang and R. Jin, *J. Am. Chem. Soc.*, 2011, **133**, 9670–9673.
33 E. S. Shibu, M. A. H. Muhammed, T. Tsukuda and T. Pradeep, *J. Phys. Chem. C*, 2008, **112**, 12168–12176.
34 W. Kurashige, M. Yamaguchi, K. Nobusada and Y. Negishi, *J. Phys. Chem. Lett.*, 2012, **3**, 2649–2652.
35 T. A. D. Nguyen, Z. R. Jones, D. F. Leto, G. Wu, S. L. Scott and T. W. Hayton, *Chem. Mater.*, 2016, **28**, 8385–8390.
36 Y. Niihori, C. Uchida, W. Kurashige and Y. Negishi, *Phys. Chem. Chem. Phys.*, 2016, **18**, 4251–4265.
37 Y. Negishi, K. Nobusada and T. Tsukuda, *J. Am. Chem. Soc.*, 2005, **127**, 5261–5270.
38 Y. Yu, Z. Luo, Y. Yu, J. Y. Lee and J. Xie, *ACS Nano*, 2012, **6**, 7920–7927.
39 Y. Yu, X. Chen, Q. Yao, Y. Yu, N. Yan and J. Xie, *Chem. Mater.*, 2013, **25**, 946–952.
40 T. Chen, Q. Yao, X. Yuan, R. R. Nasaruddin and J. Xie, *J. Phys. Chem. C*, 2017, **121**, 10743–10751.
41 Z. Luo, V. Nachammai, B. Zhang, N. Yan, D. T. Leong, D. E. Jiang and J. Xie, *J. Am. Chem. Soc.*, 2014, **136**, 10577–10580.
42 Q. Yao, T. Chen, X. Yuan and J. Xie, *Acc. Chem. Res.*, 2018, **51**, 1338–1348.
43 Q. Yao, X. Yuan, V. Fung, Y. Yu, D. T. Leong, D. E. Jiang and J. Xie, *Nat. Commun.*, 2017, **8**, 1–10.
44 M. W. Heaven, A. Dass, P. S. White, K. M. Holt, R. W. Murray, K. Laboratories, V. Uni, C. Hill and N. Carolina, *J. Am. Chem. Soc.*, 2008, **130**, 3754–3755.
45 M. Zhu, C. M. Aikens, F. J. Hollander, G. C. Schatz and R. Jin, *J. Am. Chem. Soc.*, 2008, **130**, 5883–5885.
46 S. Chen, S. Wang, J. Zhong, Y. Song, J. Zhang, H. Sheng and Y. Pei, *Angew. Chem. Int. Ed.*, 2015, **54**, 3145–3149.
47 A. Das, C. Liu, H. Y. Byun, K. Nobusada, S. Zhao, N. Rosi and R. Jin, *Angew. Chem. Int. Ed.*, 2015, **54**, 3140–3144.
48 A. Tlahuice-flores, M. Jose-Yacaman and R. L. Whetten, *Phys. Chem. Chem. Phys.*, 2013, **15**, 19557–19560.
49 Y. Pei, P. Wang, Z. Ma and L. Xiong, *Acc. Chem. Res.*, 2019, **52**, 23–33.
50 Y. Pei, J. Tang, X. Tang, Y. Huang and X. C. Zeng, *J. Phys. Chem. Lett.*, 2015, **6**, 1390–1395.
51 X. S. Han, X. Luan, H. F. Su, J. J. Li, S. F. Yuan, Z. Lei, Y. Pei and Q. M. Wang, *Angew. Chem. Int. Ed.*, 2020, **59**, 2309–2312.
52 N. Goswami, R. Bright, R. M. Visalakshan, B. Biswas, P. Zilm and K. Vasilev, *Nanoscale Adv.*, 2019, **1**, 2356–2364.

53 Y. Wang, J. J. Chen and J. Irudaraj, *ACS Nano*, 2011, **5**, 9718–9725.
54 Y. Li, P. Li, R. Zhu, C. Luo, H. Li, S. Hu, Z. Nie, Y. Huang and S. Yao, *Anal. Chem.*, 2016, **88**, 11184–11192.
55 Y. Lei, L. Tang, Y. Xie, Y. Xianyu, L. Zhang, P. Wang, Y. Hamada, K. Jiang, W. Zheng and X. Jiang, *Nat. Commun.*, 2017, **8**(15130), 1–15.
56 A. R. Girija, S. Balasubramanian, R. Bright, A. J. Cowin, N. Goswami and K. Vasilev, *ChemNanoMat*, 2019, **5**, 1176–1181.
57 Y. Tao, M. Li, J. Ren and X. Qu, *Chem. Soc. Rev.*, 2015, **44**, 8636–8663.
58 L. Zhang and E. Wang, *Nano Today*, 2014, **9**, 132–157.
59 J. M. Forward, D. Bohmann, J. P. Fackler and R. J. Staples, *Inorg. Chem.*, 1995, **34**, 6330–6336.
60 Z. Wu and R. Jin, *Nano Lett.*, 2010, **10**, 2568–2573.
61 S. Wang, X. Meng, A. Das, T. Li, Y. Song, T. Cao, X. Zhu, M. Zhu and R. Jin, *Angew. Chem. Int. Ed.*, 2014, **53**, 2376–2380.
62 X. L. Guevel, O. Tagit, C. E. Rodriguez, V. Trouillet, M. P. Leal and N. Hieldbrandt, *Nanoscale*, 2014, **6**, 8091–8099.
63 M. Walter, J. Akola, O. L-Acevedo, P. D. Jadzinsky, G. Calero, C. J. Ackerson, R. L. Whetten, H. Gronbeck and H. Hakkinen, *Proc. Natl. Acad. Sci. U. S. A.*, 2008, **105**, 9157–9162.
64 Z. Ma, P. Wang, L. Xiong and Y. Pei, *Wiley Interdiscip. Rev.: Comput. Mol. Sci.*, 2017, **7**, e1315.
65 M. J. Cowan and G. Mpourmpakis, *Nanoscale Adv.*, 2019, **1**, 184–188.
66 Y. Hong, W. Y. Lam and B. Z. Tang, *Chem. Commun.*, 2009, 4332–4353.
67 J. Mei, Y. Hong, J. W. Y. Lam, A. Qin, Y. Tang and B. Z. Tang, *Adv. Mater.*, 2014, **26**, 5429–5479.
68 Z. Luo, X. Yuan, Y. Yu, Q. Zhang, D. T. Leong, J. Y. Lee and J. Xie, *J. Am. Chem. Soc.*, 2012, **134**, 16662–16670.
69 Y. Yu, Z. Luo, D. B. Chevrier, D. T. Leong, P. Zhang, D. Jiang and J. Xie, *J. Am. Chem. Soc.*, 2014, **136**, 1246–1249.
70 L. Shang and G. U. Nienhaus, *APL Mater.*, 2017, **5**, 053101.
71 A. A. Saei, M. Yazdani, S. E. Lohse, Z. Bakhtiary, V. Serpooshan, M. Ghavami, M. Asadian, S. Mashaghi, E. C. Dreaden, A. Mashaghi and M. Mahmoudi, *Chem. Mater.*, 2017, **29**, 6578–6595.
72 J. Y. Zhao, R. Cui, Z. L. Zhang, M. Zhang, Z. X. Xie and D. W. Pang, *Nanoscale*, 2014, **6**, 13126–13134.
73 E. B. Ehlerding, F. Chen and W. Cai, *Adv. Sci.*, 2016, **3**, 1500223.
74 M. Yu, J. Xu and J. Zheng, *Angew. Chem. Int. Ed.*, 2019, **58**, 4112–4128.
75 A. E. Nel, L. Mädler, D. Velegol, T. Xia, E. M. V. Hoek, P. Somasundaran, F. Klaessig, V. Castranova and M. Thompson, *Nat. Mater.*, 2009, **8**, 543–557.
76 G. Caracciolo, O. C. Farokzad and M. Mahmoudi, *Trends Biotechnol.*, 2017, **35**, 257–264.
77 E. Casals, T. Pfaller, A. Duschl, G. J. Oostingh and V. Puntes, *ACS Nano*, 2010, **4**, 3623–3632.
78 M. Kopp, S. Kollenda and M. Epple, *Acc. Chem. Res.*, 2017, **50**, 1383–1390.
79 A. L. Lira, R. S. Ferreira, R. J. S. Torquato, M. L. V. Oliva, P. Schuck and A. A. Sousa, *Nanoscale Adv.*, 2019, **1**, 378–388.
80 D. Baimanov, R. Cai and C. Chen, *Bioconjugate Chem.*, 2019, **30**, 1923–1937.
81 C. D. Walkey and W. C. W. Chan, *Chem. Soc. Rev.*, 2012, **41**, 2780–2799.
82 A. L. Lira, R. S. Ferreira, R. J. S. Torquato, H. Zhao, M. L. Oliva, S. A. Hassan, P. Schuck and A. Sousa, *Nanoscale*, 2018, **10**, 3235–3244.
83 M. M. Yin, P. Dong, W. Q. Chen, S. P. Xu, L. Y. Yang, F. L. Jiang and Y. Liu, *Langmuir*, 2017, **33**, 5108–5116.
84 C. Zhou, M. Long, Y. Qin, X. Sun and J. Zheng, *Angew. Chem. Int. Ed.*, 2011, **50**, 3226–3230.
85 F. Alexis, E. Pridgen, L. K. Molnar and O. C. Farokhzad, *Mol. Pharm.*, 2008, **5**, 505–515.
86 S. G. Elci, Y. Jiang, B. Yan, S. T. Kim, K. Saha, D. F. Moyano, G. Yesilbag Tonga, L. C. Jackson, V. M. Rotello and R. W. Vachet, *ACS Nano*, 2016, **10**, 5536–5542.
87 J. S. Suk, Q. Xu, N. Kim, J. Hanes and L. M. Ensign, *Adv. Drug Delivery Rev.*, 2016, **99**, 28–51.
88 J. Liu, M. Yu, X. Ning, C. Zhou, S. Yang and J. Zheng, *Angew. Chem. Int. Ed.*, 2013, **52**, 12572–12576.
89 S. Huo, S. Chen, N. Gong, J. Liu, X. Li, Y. Zhao and X.-J. Liang, *Bioconjugate Chem.*, 2017, **28**, 239–243.
90 C. Y. Tay, Y. Yu, M. I. Setyawati, J. Xie and D. T. Leong, *Nano Res.*, 2014, **7**, 805–815.
91 M. Yu, C. Zhou, J. Liu, J. D. Hankins and J. Zheng, *J. Am. Chem. Soc.*, 2011, **133**, 11014–11017.
92 O. A. Wong, R. J. Hansen, T. W. Ni, C. L. Heinecke, W. S. Compel, D. L. Gustafson and C. J. Ackerson, *Nanoscale*, 2013, **5**, 10525–10533.
93 X. D. Zhang, D. Wu, X. Shen, P. X. Liu, F. Y. Fan and S. J. Fan, *Biomaterials*, 2012, **33**, 4628–4638.
94 E. Porret, L. Sancey, A. Martín-Serrano, M. I. Montañez, R. Seeman, A. Yahia-Ammar, H. Okuno, F. Gomez, A. Ariza, N. Hildebrandt, J.-B. Fleury, J.-L. Coll and X. Le Guével, *Chem. Mater.*, 2017, **29**, 7497–7506.
95 T. G. Iversen, T. Skotland and K. Sandvig, *Nano Today*, 2011, **6**, 176–185.
96 H. Yuan, J. Li, G. Bao and S. Zhang, *Phys. Rev. Lett.*, 2010, **105**, 138101.
97 C. Zhou, G. Hao, P. Thomas, J. Liu, M. Yu, S. Sun, O. K. Oz, X. Sun and J. Zheng, *Angew. Chem. Int. Ed.*, 2012, **51**, 10118–10122.
98 B. Du, M. Yu and J. Zheng, *Nat. Rev. Mater.*, 2018, **3**, 358–374.
99 B. Du, X. Jiang, A. Das, Q. Zhou, M. Yu, R. Jin and J. Zheng, *Nat. Nanotechnol.*, 2017, **12**, 1096–1102.
100 Y. Lu and Z. Gu, *Nat. Nanotechnol.*, 2017, **12**, 1023–1025.
101 X. Ning, C. Peng, E. S. Li, J. Xu, R. D. Vinluan, M. Yu and J. Zheng, *APL Mater.*, 2017, **5**, 053406.
102 M. C. Daniel and D. Astruc, *Chem. Rev.*, 2004, **104**, 293–346.
103 L. Strong and G. M. Whitesides, *Langmuir*, 1988, **4**, 546–558.
104 H. Häkkinen, *Nat. Chem.*, 2012, **4**, 443–455.

105 X. Yuan, B. Zhang, Z. Luo, Q. Yao, D. T. Leong, N. Yan and J. Xie, *Angew. Chem. Int. Ed.*, 2014, **53**, 4623–4627.
106 J. M. Abad, S. F. L. Mertens, M. Pita, V. M. Fernández and D. J. Schiffrin, *J. Am. Chem. Soc.*, 2005, **127**, 5689–5694.
107 F. Aldeek, M. A. H. Muhammed, G. Palui, N. Zhan and H. Mattoussi, *ACS Nano*, 2013, **7**, 2509–2521.
108 J. Xie, Y. Zheng and J. Y. Ying, *J. Am. Chem. Soc.*, 2009, **131**, 888–889.
109 L. Wang, X. Jiang, M. Zhang, M. Yang, Y. Liu, L. Wang, X. Jiang, M. Zhang, M. Yang and Y. N. Liu, *Chem. – Asian J.*, 2017, **12**, 2374–2378.
110 K. Shanmugaram and M. Ilanchelian, *RSC Adv.*, 2016, **6**, 54518–54524.
111 H. Kawasaki, K. Hamaguchi, R. Osaka and I. Arakawa, *Adv. Funct. Mater.*, 2011, **21**, 3508–3515.
112 C. L. Liu, H. T. Wu, Y. H. Hsiao, C. W. Lai, C. W. Shih, Y. K. Peng, K. C. Tang, H. W. Chang, Y. C. Chien, J. K. Hsiao, J. T. Cheng and P. T. Chou, *Angew. Chem. Int. Ed.*, 2011, **50**, 7056–7060.
113 Q. Q. Zhuang, H. H. Deng, S. B. He, H. P. Peng, Z. Lin, X. H. Xia and W. Chen, *ACS Appl. Mater. Interfaces*, 2019, **11**, 31729–31734.
114 A. Aires, I. Llarena, M. Moller, J. Castro-Smirnov, J. Cabanillas-gonzalez and A. L. Cortajarena, *Angew. Chem. Int. Ed.*, 2019, **58**, 6214–6219.
115 K. Chaudari, P. L. Xavier and T. Pradeep, *ACS Nano*, 2011, **5**, 8816–8827.
116 D. Ghosh, A. Baksi, S. K. Mudedla, A. Nag, M. A. Ganayee, V. Subramanian and T. Pradeep, *J. Phys. Chem. C*, 2017, **121**, 13335–13344.
117 D. Ghosh, S. K. Mudedla, M. R. Islam, V. Subramanian and T. Pradeep, *J. Phys. Chem. C*, 2019, **123**, 17598–17605.
118 M. J. Pallardy, I. Turbica and A. Biola-Vidamment, *Front. Immunol.*, 2017, **8**(544), 1–6.
119 M. Hembury, N. Beztsinna, H. Asadi, J. B. Van Den dikkenberg, J. D. Meeldijk, W. E. Hennink and T. Vermonden, *Biomacromolecules*, 2018, **19**, 2841–2848.
120 B. Santiago González, M. J. Rodríguez, C. Blanco, J. Rivas, M. A. López-Quintela and J. M. G. Martinho, *Nano Lett.*, 2010, **10**, 4217–4221.
121 Y. Tao, Z. Li, E. Ju, J. Ren and X. Qu, *Nanoscale*, 2013, **5**, 6154–6160.
122 F. Grohn, B. J. Bauer, Y. A. Akpalu, C. L. Jackson and E. J. Amis, *Macromolecules*, 2000, **33**, 6042–6050.
123 J. Zheng, J. T. Petty and R. M. Dickson, *J. Am. Chem. Soc.*, 2003, **125**, 7780–7781.
124 J. K. Vohs and B. D. Fahlman, *New J. Chem.*, 2007, **31**, 1041–1051.
125 L. Yang, H. Wang, D. Li, L. Li, X. Lou and H. Liu, *Chem. Mater.*, 2018, **30**, 5507–5515.
126 M. J. Hostetler, A. C. Templeton and R. W. Murray, *Langmuir*, 1999, **15**, 3782–3789.
127 Y. Shichibu, Y. Negishi, T. Tsukuda and T. Teranishi, *J. Am. Chem. Soc.*, 2005, **127**, 13464–13465.
128 A. George, A. Sundar, A. S. Nair, M. P. Maman, B. Pathak, N. Ramanan and S. Mandal, *J. Phys. Chem. Lett.*, 2019, **10**, 4571–4576.
129 G. S. Yuvasri, N. Goswami and J. Xie, in *Princinples and Applications of Aggregation-Induced Emission*, ed. Y. Tang and B. Z. Tang, Springer, Cham, 2019, pp. 265–289.
130 Z. Wu, Y. Du, J. Liu, Q. Yao, T. Chen, Y. Cao, H. Zhang and J. Xie, *Angew. Chem., Int. Ed.*, 2019, **58**, 8139–8144.
131 Z. Wu, Q. Yao, O. J. H. Chai, N. Ding, W. Xu, S. Zang and J. Xie, *Angew. Chem., Int. Ed.*, 2020, **59**, 9934–9939.
132 X. Dou, X. Yuan, Y. Yu, Z. Luo, Q. Yao, D. T. Leong and J. Xie, *Nanoscale*, 2014, **6**, 157–161.
133 K. Pyo, V. D. Thanthirige, K. Kwak, P. Pandurangan, G. Ramakrishna and D. Lee, *J. Am. Chem. Soc.*, 2015, **137**, 8244–8250.
134 K. Pyo, V. D. Thanthirige, S. Y. Yoon, G. Ramakrishna and D. Lee, *Nanoscale*, 2016, **8**, 20008–20016.
135 K. Pyo, N. H. Ly, S. Y. Soon, Y. Shen, S. Y. Choi, S. Y. Lee, S. Joo and D. Lee, *Adv. Healthcare Mater.*, 2017, **6**, 1700203.
136 G. M. Whitesides, J. P. Mathias and C. T. Seto, *Science*, 1991, **254**, 1312–1319.
137 G. M. Whitesides, *Science*, 2002, **295**, 2418–2421.
138 C. Stoffelen and J. Huskens, *Small*, 2016, **12**, 96–119.
139 N. Goswami, F. Lin, Y. Liu, D. T. Leong and J. Xie, *Chem. Mater.*, 2016, **28**, 4009–4016.
140 A. Yahia-Ammar, D. Sierra, F. Mérola, N. Hildebrandt and X. Le Guével, *ACS Nano*, 2016, **10**, 2591–2599.
141 F. Cao, E. Ju, C. Liu, W. Li, Y. Zhang, K. Dong, Z. Liu, J. Ren and X. Qu, *Nanoscale*, 2017, **9**, 4128–4134.
142 L. Zhang, Y. Gao, S. Sun, Z. Li, A. Wu and L. Zhang, *J. Mater. Chem. B*, 2020, **8**, 1739–1747.
143 X. Wu, L. Li, L. Zhang, T. Wang, C. Wang and Z. Su, *J. Mater. Chem. B*, 2015, **3**, 2421–2425.
144 J. G. Croissant, D. Zhang, S. Alsaiari, J. Lu, L. Deng, F. Tamanoi, A. M. Almalik, J. I. Zink and N. M. Khashab, *J. Controlled Release*, 2016, **229**, 183–191.
145 H. Gao, W. Shi and L. B. Freund, *Proc. Natl. Acad. Sci. U. S. A.*, 2005, **102**, 9469–9474.
146 C. Zhang, A. Zhang, W. Hou, T. Li, K. Wang, Q. Zhang, J. M. De La Fuente, W. Jin and D. Cui, *ACS Nano*, 2018, **12**, 4408–4418.
147 D. J. Cram and J. M. Cram, *Science*, 1974, **183**, 803–809.
148 G. Sinawang, M. Osaki, Y. Takashima, H. Yamaguchi and A. Harada, *Chem. Commun.*, 2020, **56**, 4381–4395.
149 H.-J. Scheneider, *Angew. Chem. Int. Ed.*, 2009, **48**, 3924–3977.
150 O. Livnah, E. A. Bayer, M. Wilchek and J. L. Sussman, *Proc. Natl. Acad. Sci. U. S. A.*, 1993, **90**, 5076–5080.
151 M. V. Rekarsky, T. More, C. Yang, H. K. Young, N. Selvapalam, H. Kim, D. Sobrasingh, A. E. Kaifer, S. Liu, L. Isaacs, W. Chen, S. Moghadam, M. K. Gilson, O. Kim and Y. Inoue, *Proc. Natl. Acad. Sci. U. S. A.*, 2007, **104**, 20737–20742.
152 T. Chen, Y. Hu, Y. Cen, X. Chu and Y. Lu, *J. Am. Chem. Soc.*, 2013, **135**, 11595–11602.
153 X. Jiang, X. Wang, C. Yao, S. Zhu, L. Liu, R. Liu and L. Li, *J. Phys. Chem. Lett.*, 2019, **10**, 5237–5243.

154 Q. Li, Y. Pan, T. Chen, Y. Du, H. Ge, B. Zhang, J. Xie, H. Yu and M. Zhu, *Nanoscale*, 2018, **10**, 10166–10172.
155 U. Gerhard, J. P. Mackay, R. A. Maplestone and D. H. Williams, *J. Am. Chem. Soc.*, 1993, **115**, 232–237.
156 H. Zhu, N. Goswami, Q. Yao, T. Chen, Y. Liu, Q. Xu, D. Chen, J. Lu and J. Xie, *J. Mater. Chem. A*, 2018, **6**, 1102–1108.
157 R. Ban, E. S. Abdel- Halim, J. Zhang and J.-J. Zhu, *Analyst*, 2015, **140**, 1046–1053.
158 Q.-D. Hu, G.-P. Tang and P. K. Chu, *Acc. Chem. Res.*, 2014, **47**, 2017–2025.
159 C. Yan, C. Liu, H. Abroshan, Z. Li, R. Qiu and G. Li, *Phys. Chem. Chem. Phys.*, 2016, **18**, 23358–23364.
160 D. Chen, Z. Luo, N. Li, J. Y. Lee, J. Xie and J. Lu, *Adv. Funct. Mater.*, 2013, **23**, 4324–4331.
161 J. Qiao, X. Mu, L. Qi, J. Deng and L. Mao, *Chem. Commun.*, 2013, **49**, 8030–8032.
162 R. Vankayala, C. L. Kuo, K. Nuthalapati, C. S. Chiang and K. C. Hwang, *Adv. Funct. Mater.*, 2015, **25**, 5934–5945.
163 D. Chen, B. Li, S. Cai, P. Wang, S. Peng, Y. Sheng, Y. He, Y. Gu and H. Chen, *Biomaterials*, 2016, **100**, 1–16.
164 A. Latorre, A. Latorre, M. Castellanos, C. R. Diaz, A. Lazora-Carrillo, T. Aguado, M. Lecea, S. Romero-Perez, M. Calero, J. M. Sanchez-Puelles and A. Villanueva, *Cancers*, 2019, **11**(969), 1–17.
165 M. Yamamoto, K. Shitomi, S. Miyata, H. Miyaji, H. Aota and H. Kawasaki, *J. Colloid Interface Sci.*, 2018, **510**, 221–227.
166 W. Zhao, Z. Wang, L. Chen, C. Huang, Y. Huang and N. Jia, *Mater. Sci. Eng., C*, 2017, **78**, 565–570.
167 C. Ding, Y. Xu, Y. Zhao, H. Zhong and X. Luo, *ACS Appl. Mater. Interfaces*, 2018, **10**, 8947–8954.
168 D. Pallorola, A. Bochen, H. Boehm, F. Rechenmacher, T. R. Sobahi, J. P. Spatz and H. Kessler, *Adv. Funct. Mater.*, 2014, **24**, 943–956.
169 Y. Wang, W. Xiao, Y. Zhang, L. Meza, H. Tseng, Y. Takada, J. B. Ames and K. S. Lam, *Mol. Cancer Ther.*, 2016, **15**, 232–240.
170 R. Weissleder, *Science*, 2006, **312**, 1168–1172.
171 W. Wang, Z. Ma, S. Zhu, H. Wan, J. Yue, H. Ma, R. Ma, Q. Yang, Z. Wang, Q. Li, Y. Qian, C. Yue, Y. Wang, L. Fan, Y. Zhong, Y. Zhou, H. Gao, J. Ruan, Z. Hu, Y. Liang and H. Dai, *Adv. Mater.*, 2018, **30**, e1800106.
172 S. Santra, H. Yang, P. H. Holloway, J. T. Stanley and R. A. Mericle, *J. Am. Chem. Soc.*, 2005, **127**, 1656–1657.
173 J. M. Chem, Q. Zhao, K. Li, S. Chen, A. Qin, D. Ding, S. Zhang, Y. Liu, B. Liu, J. Z. Sun and B. Z. Tang, *J. Mater. Chem.*, 2012, **22**, 15128–15135.
174 A. M. Derfus, W. C. M. Chan and S. N. Bhatia, *Nano Lett.*, 2004, **4**, 11–18.
175 C. Dai, C. Yang and X. Yan, *Nano Res.*, 2018, **11**, 2488–2497.
176 Y. Zheng, W. Liu, Y. Chen, H. Jiang and X. Wang, *J. Mater. Chem. B*, 2018, **6**, 3650–3654.
177 R. T. Gordon, *US Pat.*, US4136683A, 1977.
178 J. Ye, X. Dong, H. Jiang and X. Wang, *J. Mater. Chem. B*, 2017, **5**, 691–696.
179 S. Kundu, D. Mukherjee, T. K. Maiti and N. Sarkar, *ACS Appl. Bio. Mater.*, 2019, **2**, 2078–2091.
180 Y. Liu, X. Lv, H. Liu, Z. Zhou, J. Huang, S. Lei, S. Cai, Z. Chen, Y. Guo, Z. Chen, X. Zhou and L. Nie, *Nanoscale*, 2018, **10**, 3631–3638.
181 B. Musnier, K. D. Wegner, C. C. Zerbino, V. Trouillet, M. Jourdan, I. Hausler, R. Antoine, J.-L. Coll, U. R. Genger and X. L. Guevel, *Nanoscale*, 2019, **11**, 12092–12096.
182 H. Liu, G. Hong, Z. Luo, J. Chen, M. Gong, H. He, J. Yang, X. Yuan, L. Li, X. Mu, J. Wang, W. Mi, J. Luo, J. Xie and X.-D. Zhang, *Adv. Mater.*, 2019, **31**, e1901015.
183 Z. Xu, X. Chen, Z. Sun, C. Li and B. Jiang, *Mater. Today. Chem.*, 2019, **12**, 240–260.
184 Y. Yang, S. Wang, S. Chen, Y. Shen and M. Zhu, *Chem. Commun.*, 2018, **54**, 9222–9225.
185 J. Zhai, Y. Jia, L. Zhao, Q. Yuan, F. Gao, X. Zhang, P. Cai, L. Gao, J. Guo, S. Yi, Z. Chai, Y. Zhao and X. Gao, *ACS Nano*, 2018, **12**, 4378–4386.
186 Z. Li and K. B. Grant, *RSC Adv.*, 2016, **6**, 24617–24634.
187 P. Mroz, A. Yaroslavsky, G. B. Kharkwal and M. R. Hamblin, *Cancers*, 2011, **3**, 2516–2539.
188 B. Knap, D. Przystupski, J. Saczko, K. Ewa, K. Knap-czop, J. Kotli, O. Michel, K. Kotowski and J. Kulbacka, *Biomed. Pharm.*, 2018, **106**, 1098–1107.
189 X. Wen, P. Yu, Y. Toh, A. Hsu, Y. Lee and J. Tang, *J. Phys. Chem. C*, 2012, **116**, 19032–19038.
190 T. Das, P. Ghosh, M. S. Shanavas, A. Maity, S. Mondal and P. Purkayastha, *Nanoscale*, 2012, **4**, 6018–6024.
191 H. Kawasaki, S. Kumar, G. Li, C. Zeng, D. R. Kau, J. Yoshimoto, Y. Iwasaki and R. Jin, *Chem. Mater.*, 2014, **26**, 2777–2788.
192 M. Sakamoto, T. Tachikawa, M. Fujitsuka and T. Majima, *Langmuir*, 2009, **25**, 13888–13893.
193 R. Ho-wu, S. H. Yau and T. Goodson, *J. Phys. Chem. B*, 2017, **121**, 10073–10080.
194 L. V. Nair, S. S. Nazeer, R. S. Jayasree and A. Ajayaghosh, *ACS Nano*, 2015, **9**, 5825–5832.
195 J. Xia, X. Wang, S. Zhu, L. Liu and L. Li, *ACS Appl. Mater. Interfaces*, 2019, **11**, 7369–7378.
196 Q. Chen, J. Chen, Z. Yang, L. Zhang, Z. Dong and Z. Liu, *Nano Res.*, 2018, **11**, 5657–5669.
197 A. P. Castano, P. Mroz and M. R. Hamblin, *Nat. Rev. Cancer*, 2006, **6**, 535–545.
198 W. Yu, X. He, Z. Yang, X. Yang, W. Xiao, R. Liu, R. Xie, L. Qin and H. Gao, *Biomaterials*, 2019, **217**, 119309.
199 M. Bjo, K. J. Thurecht, M. Michael, A. M. Scott and F. Caruso, *ACS Nano*, 2017, **11**, 9594–9613.
200 R. Baskar, K. A. Lee, R. Yeo and K. W. Yeoh, *Int. J. Med. Sci.*, 2012, **9**, 193–199.
201 H. Wang, H. Jiang, M. Van De Gucht and M. De Ridder, *Cancer*, 2019, **11**(112), 1–23.
202 H. E. Barker, J. T. Paget, A. A. Khan and K. J. Harrington, *Nat. Rev. Cancer*, 2015, **15**, 409–425.
203 X. D. Zhang, Z. Luo, J. Chen, X. Shen, S. Song, Y. Sun, S. Fan, F. Fan, D. T. Leong and J. Xie, *Adv. Mater.*, 2014, **26**, 4565–4568.
204 X.-D. Zhang, J. Chen, Z. Luo, D. Wu, X. Shen, S.-S. Song, Y.-M. Sun, P.-X. Liu, J. Zhao, S. Huo, S. Fan, F. Fan, X.-J. Liang and J. Xie, *Adv. Healthcare Mater.*, 2014, **3**, 133–141.

205 M. Broekgaarden, A.-L. Bulin, E. Porret, B. Musnier, B. Chovelon, C. Ravelet, L. Sancey, H. Elleaume, P. Hainaut, J.-L. Coll and X. L. Guevel, *Nanoscale*, 2020, **12**, 6959–6963.
206 D. Luo, X. Wang, S. Zeng, G. Ramamurthy, C. Burda and J. P. Basilion, *Small*, 2019, **15**, 1900968.
207 J. Chen, Q. Chen, C. Liang, Z. Yang, L. Zhang, X. Yi, Z. Dong, Y. Chao, Y. Chen and Z. Liu, *Nanoscale*, 2017, **9**, 14826–14835.
208 L. J. V. Piddock, *Lancet Infect. Dis.*, 2012, **12**, 249–253.
209 A. J. Huh and Y. J. Kwon, *J. Controlled Release*, 2011, **156**, 128–145.
210 L. R. Morones, J. L. Elechiguerra, A. Camacho, K. Holt, J. B. Kouri, J. T. Ramirez and M. J. Yacaman, *Nanotechnology*, 2005, **16**, 2346–2353.
211 K. Zheng, M. I. Setyawati, D. T. Leong and J. Xie, *Coord. Chem. Rev.*, 2018, **357**, 1–17.
212 K. Zheng and J. Xie, *Trends Chem.*, 2020, **2**, 665–679.
213 K. Zheng, M. I. Setyawati, D. T. Leong and J. Xie, *Chem. Mater.*, 2018, **30**, 2800–2808.
214 Y. Xie, Y. Liu, J. Yang, Y. Liu, F. Hu, K. Zhu and X. Jiang, *Angew. Chem. Int. Ed.*, 2018, **57**, 3958–3962.
215 D. Pranantyo, P. Liu, W. Zhong, E.-T. Kanmg and M. B. Chan-Park, *Biomacromolecules*, 2019, **20**, 2922–2933.
216 R. Yin, T. Agrawal, U. Khan, G. K. Gupta, V. Rai, Y. Y. Huang and M. R. Hamblin, *Nanomedicine*, 2015, **10**, 2379–2404.
217 B. Khlebtsov, E. Tuchina, V. Tuchin and N. Khlebtsov, *RSC Adv.*, 2015, **5**, 61639–61649.
218 K. Zheng, K. Li, T. Chang, J. Xie and P. Chen, *Adv. Funct. Mater.*, 2019, **29**, 1904603.

